HOKKAIDO UNIVERSITY

Title	Bed instability in suspended load-dominated environments
Author(s)	Pen, Sytharith
Degree Grantor	北海道大学
Degree Name	博士(工学)
Dissertation Number	甲第13212号
Issue Date	2018-03-22
DOI	https://doi.org/10.14943/doctoral.k13212
Doc URL	https://hdl.handle.net/2115/69997
Type	doctoral thesis
File Information	Pen_Sytharith.pdf

Hokkaido University Collection of Scholarly and Academic Papers : HUSCAP

Bed instability in suspended load-dominated environments

PEN Sytharith

A thesis submitted in partial fulfillment of the requirements for the degree of
Doctor of Engineering

Examination Committee:

Prof. Norihiro IZUMI
Prof. Yasuyuki SHIMIZU
Prof. Toshihiko YAMASHITA

Doctoral Thesis No. EG-M...
Division of Field Engineering for the Environment
Graduate School of Engineering, Hokkaido University
March 2018

Abstract

The bed instability of stratified open channel flow and turbidity currents is investigated in this study. The first setting is free surface flow in a channel with dominant suspended sediment load, and the second is a turbidity current on the ocean floor the movement of which is driven by suspended sediment.

A linear stability analysis is performed in order to investigate the bed instability of open channel flow. The bed is assumed to be covered with sediment. The sediment is assumed to be so fine as to completely follow the flow except it sinks at a settling velocity in the vertical direction. The governing equations are the two-dimensional Reynolds-averaged Navier-Stokes equations (RANS) and the dispersion/diffusion equation of suspended sediment. In addition, as a turbulent closure model, we employ the standard k-ϵ model which includes the transport equations of the turbulent kinetic energy and the dissipation rate.

The open channel flow is assumed to be in the upper flow regime, and dominated by suspended sediment with bedload being negligible. As far as suspended load is concerned, density stratification is an important factor as it affects internal structures of turbulence, and changes the flow velocity and the suspended sediment concentration. Therefore, density stratification is expected to affect the stability of the bed under free surface flow with dominant suspended sediment load. The base state is assumed to be in an equilibrium condition. Under this condition, all the variables are uniform in the streamwise direction and the vertical component of velocity vanishes. The equations in the base state are solved numerically by the use of a finite control volume method.

It is found that the density stratification increases the flow velocity in the upper depth region, and increases the suspended sediment concentration near the bottom. The mixing capacity due to turbulence is reduced under the density stratification as reflected in the decrease of the eddy viscosity. In the perturbation problem, the asymptotic expansion of the variables are then introduced into the governing equations to obtain the perturbation equations. Because the perturbation equations cannot be solved analytically, they are solved by a numerical scheme. The spectral collocation method incorporated with the Chebyshev polynomials are used to solve the perturbation equations. Substituting the solutions into the Exner equation, the growth rate of perturbation is obtained.

The results of the analysis are illustrated in instability diagrams. The antidunes are found to form in the upper flow regime. The instability regions predicted by the analysis are fairly reasonable as the experimental results fall almost all in the

instability regions. Under the density stratification effect, the instability region of antidune is shifted to the range of smaller wavenumbers, which is corresponding to the range of longer wavelengths, around the critical Froude number. In addition, this analysis also shed light on the migration mechanism of the antidunes. The model predicts that antidunes could migrate in both the upstream and downstream directions. The mechanism of the migration is explained by the phase shift between the bed elevation and the net erosion rate. For the upstream migrating antidunes, the net erosion rate reaches maximum (minimum) slightly upstream of the trough (crest) of the bed waves. This process implies that the wave amplitude increases and the waves migrate in the upstream direction. In the case of downstream migrating antidunes, increases in the amplitude of bed waves is governed by the same process as that of the upstream migrating antidunes, however, the maximum (minimum) of the erosion rate takes place slightly downstream of the trough (crest) of the bed waves. Thus, the bed waves migrate in the downstream direction.

Instability generated under turbidity currents is studied. A turbidity current is a density flow the driving force of which is a density increase due to suspended sediment contained in water. In the case of saline or thermal density flows, salt concentration or temperature as driving force is diluted due to diffusion as it flows down, and therefore, it cannot move long distance. In the case of turbidity currents however, it has been found that the lower layer with high sediment concentration has an equilibrium state because the diffusion is balanced with the settling of suspended sediment.

In the analysis of turbidity currents, the two-dimensional Reynolds-averaged Navier-Stokes equations are used with the Boussinesq approximation. Because the suspended sediment is the dominant driving force of turbidity currents, the suspended sediment concentration appears in the momentum equations. In addition, the dispersion/diffusion equation of suspended sediment is employed. As a turbulent closure, the mixing length hypothesis is used to evaluate the eddy viscosity. In the base state condition, the flow velocity is affected by the suspended sediment concentration. As the sediment settling velocity increases, the suspended sediment concentration is reduced in the upper depth region, and emphasized in the lower depth region, resulting in a decrease and an increase in the flow velocity in the upper and lower depth regions, respectively. Meanwhile, as the sediment settling velocity decreases, the suspended sediment concentration becomes relatively uniform, resulting in the velocity profile similar to that in open channel flow.

As a result of the linear stability analysis of bed instability under turbidity currents, it is found that the flat bed becomes unstable to evolve into a bed

covered with bed waves in the range of densimetric Froude number larger than approximately 0.4. In the condition of small settling velocities, the instability region in the case of turbidity currents resembles that in open channel flow. In addition, the instability region is affected also by the settling velocity non-dimensionalized by the friction velocity in the base state. For the non-dimensional settling velocity larger than 0.08, the instability region shows a strange shape. It is suggested that turbidity currents do not have normal flow conditions under the condition of sufficiently coarse suspended sediment.

Contents

Contents **5**

List of Figures **7**

1 Introduction **9**

2 Bed instability including the effect of density stratification **17**

2.1 Introduction 17

2.2 Formulation 18

2.2.1 Flow equations 18

2.2.2 Suspended sediment model 20

2.2.3 k-ϵ model 22

2.2.4 Mixing length model 23

2.2.5 Normalization 24

2.3 Base state solution 26

2.3.1 k-ϵ model 26

2.3.2 Mixing model 31

2.3.3 Result in steady equilibrium state 33

2.4 Linear stability analysis 34

2.4.1 Perturbation expansion 36

2.4.2 General boundary conditions in perturbation problem 36

2.4.3 Solution of perturbation problem 40
2.5 Results and discussion 43
2.5.1 Characteristics of bed instability 43
2.5.2 Migration direction of antidunes 43
2.5.3 Density stratification effect 48
2.6 Conclusion 49

3 Bed instability generated by turbidity current 53
3.1 Introduction 53
3.2 Equilibrium condition of turbidity currents 54
3.3 Formulation 56
3.3.1 Flow equation 56
3.3.2 Sediment transport equation 58
3.3.3 Normalization 58
3.4 Base state solution 60
3.5 Linear stability analysis 63
3.5.1 Perturbation expansion 63
3.5.2 Boundary conditions of the perturbation problem 64
3.5.3 Solution of perturbation problem 65
3.6 Results and discussion 67
3.7 Conclusion 69

4 Conclusions 75

Bibliography 79

List of Figures

2-1 Base flow configuration 19

2-2 Base state flow velocity 34

2-3 Base state concentration 35

2-4 Base state eddy viscosity 35

2-5 Perturbation flow configuration 37

2-6 Stability diagram. Kennedy's experiment: •, d_m=0.549mm upstream migration antidune; ▲, d_m=0.549mm downstream migration antidune; ∘, d_m=0.233mm upstream migration antidune. 44

2-7 Upstream migrating antidunes (F=1.5, α=0.4).Bed elevation(solid line), net erosion(dashed line) 45

2-8 Downstream migrating antidue (F=1.5, α=0.6). Bed elevation (solid line), net erosion(dashed line) 46

2-9 Instability diagram: (a) k-ϵ model: solid line, with density stratification; dashed line, without density stratification; (b): solid line, k-ϵ model; dot-dashed line, mixing length model 47

2-10 Stability diagram of k-ϵ model $v_s = 0.2$(solid line) and $v_s = 0.1$(dashed line) 47

3-1 Conceptual flow of turbidity current in normal state condition . . . 54

3-2 Coordinate and conceptual diagram of the high concentration lower layer 57
3-3 Flow velocity profile in the base state condition 62
3-4 Suspended sediment concentration profile in the base state condition 62
3-5 Bed instability diagram generated by turbidity current (a) $v_s = 0.01$, (b) $v_s = 0.02$, (c) $v_s = 0.04$, (d) $v_s = 0.08$. 68
3-6 Instability diagram in open channel. (a) $v_s = 0.01$, (b) $v_s = 0.04$ . . 70

Chapter 1

Introduction

Bed wave formation on the bed and on the floor of the river and ocean is one of the most interesting subjects of morphology. In this study, we investigate the bed instability of the two configurations, the stratified open channel flows and the turbidity currents.

In an open channel flow, the bed and the flow are subject to instability. This instability is due to the interaction between the flowing water and the bed morphology. Under proper conditions, the bed evolves into a train of boundary waves such as ripples, dunes, and antidunes. Ripples and dunes are bedforms typically appearing in the lower flow regime, while antidunes are those observed in the upper flow regime. These bed features are not only growing in magnitude, but are also migrating either upstream or downstream. Dunes usually migrate in the downstream direction, whereas antidunes migrate in both upstream and downstream directions, respectively.

Since the seminal work of Kennedy [1963], the theory of instability which described and showed that the formation of dunes and antidunes in erodible bed

is due to the instability mechanism, there are some important theoretical models, based on linear stability analyses, which predict the temporal growth or decay of the bed morphology.

Engelund [1970] used the vorticity transport equation to study the bed stability of an alluvial channel. In the condition of high flow rate and relatively fine sediment, the flow is dominated by suspended sediment, and the bedload is negligible. Thus, in this condition, the total sediment transport rate is basically the suspended sediment load, and as a result the dunes vanish while only antidunes are subject to instability observed in the upper flow regime. Further analysis by including the bedload to cover the low flow regime revealed that the dunes are found to form in the range of subcritical flow.

Fredsoe [1974] continued and elaborated the formulation of Engelund [1970] to include the effect of gravity on the sediment that resists the transport of sediment particle at the stoss side and favors at the downsloping lee side of the bedwaves. The result showed that the unstable region changes remarkably for dunes but not in the antidunes region. According to Fredsoe [1974], it was suggested that the formation of antidunes is closely related to the presence of suspended sediment.

In both analyses, Engelund [1970] and Fredsoe [1974] employed the eddy viscosity concept; however, the constant value eddy viscosity was taken to be proportional to friction velocity and flow depth. This assumption is considered to be crude in the sense that it fails to describe the stratification effect due to the presence of suspended sediment.

Richards [1980] used one equation turbulent closure to account for the non-

constant eddy viscosity concept which is different from that of Engelund [1970] and Fredsoe [1974]. This concept is advancing the previous study in the sense that it is expected to provide a more realistic description of turbulence especially in the bed region. Richards [1980] restricted the analysis to low flow regime that allows only the bedload transport to be considered. However, the model does not cover the effect of suspended sediment to the bedwave formation process.

Recently, Colombini [2004] studied the instability of the bed by including only the bedload as sediment load. Mixing length hypothesis was used to evaluate the eddy viscosity, and the flow velocity is the logarithmic profile of uniform flow over flat bed. Linear stability analysis was performed to study instability of the bed. It was found that antidunes are observed to form even in a no-suspended sediment case. It was also found that the gravity has minor effects on the instability of the antidunes.

As shown by Engelund [1970] and Fredsoe [1974], the bed becomes unstable in the upper flow regime under the condition of active suspended load. Colombini's study, however, does not shed further light on bed instability under the condition of active suspended load. In this regards, we perform linear stability analysis of bed instability due to suspended sediment of an open channel flow.

In this study, we consider an open channel the flow of which is assumed to be under the upper flow regime condition. Under this consideration the suspended load is dominant and the bedload is negligible. The suspended sediment is assumed to completely followed the velocity of the flow except the sediment settling velocity in the vertical direction. As far as suspended sediment is concerned, the flow is subject to density stratification induced by the presence of suspended sediment. In

the case of suspended load being dominant, the effect of density stratification of suspended sediment is important in the way it affects the flow velocity, suspended sediment concentration, the turbulent kinetic energy, and the dissipation rate of turbulent kinetic energy (Coleman [1986], Winterwerp [2001], Winterwerp [2006], and Yeh and Parker [2013]). In addition, these changes influence the formation of the bedwaves. Therefore, it is important to investigate the effect of the density stratification to the formation of the bedwaves.

In order to investigate the effect of density stratification due to suspended sediment, the sediment transport model is assumed to be solely suspended sediment entrained by the flow. In the formulation, we employed four governing equations: the equation of the stream function ψ derived from the Reynolds-averaged Navier–Stokes equations and the dispersion/ diffusion equations of suspended sediment concentration c. For turbulent closure, the simple mixing length model and the two-equation turbulent closure (standard k-ϵ model) which includes the turbulent kinetic energy k, and the dissipation rate of the turbulent kinetic energy ϵ are used. The effect of density stratification on the bed instability analysis is investigated which, to the authors' understanding, is not yet available.

Another setting of stratified flow is the turbidity currents which occur naturally in the ocean, lake, reservoir, and dam, etc. Turbidity current is the current driven by the gravitational force on the suspended sediment in the flow. The sediment is considered to be suspended by the fluid turbulence (Lowe [1982], Middleton [1993]). This kind of current is different from other density currents by the tendency to settle down of the suspended particles in the depth direction. Normally, the current dissipates when there is no more sediment in suspension.

The turbidity current is an important agent that distributes and transports much amount of sediment in the subaqueous environments. A single turbidity current is capable of transporting hundreds of cubic kilometers of sediment into the deep ocean. This amount of sediment is approximately equal to 10 times the annual total sediment transported by all the rivers on Earth into the ocean (Talling et al. [2007c]).

In the context of sedimentology and geophysics, the sediment which is rich in organic matter and mineral is transported from the shallow region of the continental shelf to the deep ocean environment by turbidity currents (Kneller and Buckee [2000], Sequeiros et al. [2009]). Turbidity currents are generally generated by the failure of the continental shelf due to any seismic events (Weaver et al. [1992], Garcia and Hull [1994]) or storm surge, generating a surge-type currents, or ignited by the direct sediment transport by the river (Wright et al. [1990]).

In the case of saline or thermal density flow, salt concentration or temperature as a driving force is diluted due to diffusion as it flows down, and therefore, it cannot travel to distance from its source of origin without any external forces acting on it. Unlike other density currents, there are observational evidences which show that turbidity current is able to travel hundreds of kilometers at the speed range of tens of meters per second (Heezen and Ewing [1952]) before total dissipation and deposition on the seabed.

The turbidity currents are not mass-conserved as the currents evolve downstream, at least as a whole (Kneller and Buckee [2000]). The flow loses and gains the sediment to and from the sediment bed through deposition and entrainment processes. The turbidity currents also entrain the ambient fluid from the upper

boundary and reduce the driving force generated by the density difference of the currents due to suspended sediment and the ambient fluid.

However, Bagnold [1962] provided a necessary condition for the turbidity currents to be able to sustain itself against the settling tendency of the sediment and the drag force generated at the boundary. In this case, it is the power of the tangential gravitational force exerted on the sediment that keeps the sediment in suspension, and maintains the flow against the shear stress at the bottom. It is found that this criterion is met as long as the slope is sufficiently high, at which the turbidity currents are auto-suspending. Under this condition, the turbidity current is capable of entraining more sediment into suspension and travel far distance from the seashore. In addition, Parker [1982] emphasized the importance of the entrainment and deposition mechanism. The term "ignition condition" is proposed the implication of which is that there exists a set of threshold value of velocity and concentration above which the currents grow temporally and spatially.

Under certain circumstances, the turbidity current is capable of self-accelerating Parker et al. [1986]. It is believed that this self-accelerated mechanism of the turbidity current is the mechanism that transports turbidite several kilometers into the deep ocean (Parker [1982], Parker et al. [1986]). Due to this mechanism, there is a strong implication that the turbidity current plays an important role in sediment transport and morphodynamics process of the deep ocean bed, giving rise to various topographical features in the submarine environments including subaqueous abyssal fans and deltas, cyclic step, submarine canyons and gullies (Izumi [2004]), etc.

These various subaqueous morphological structures have been examined and

reported due to the advancing seafloor surveying technology. In addition to these direct evidences of the capability of the turbidity current to shape the seafloor and to travel long distance into the ocean, Luchi et al. [2015] performed a numerical analysis by adopting the concept of turbidity current with a roof (Cantero et al. [2009]) and found that the vertical structure of the turbidity currents can be partitioned into two layers, namely the bottom "driving layer" and the upper "driven layer". The upper driven layer is affected by the increase of the height of the roof, whereas the bottom driving layer is independent of the driven layer and reaches asymptotic behavior with relatively constant thickness, velocity profile, and suspended sediment concentration profile.

Based on the above result, we assume that the turbidity currents possess equilibrium condition at least at the relatively thin layer near the bottom. In this study, we perform linear stability analysis to investigate the bed instability generated by turbidity current.

Chapter 2

Bed instability including the effect of density stratification

2.1 Introduction

Suspended sediment particles in a channel flow stratify the flow by their tendency to settle down. Under the effect of stratification, the flow characteristics (e.g. flow velocity, flow depth, and flow resistance coefficient) and morphodynamics of the channel bed may be affected accordingly. Therefore, it is necessary to study the effect of density stratification on the instability of the bed in an open channel.

As a turbulent closure, the mixing length model and the standard k-ϵ model are used. The standard k-ϵ is capable of capturing the density stratification effect. Density stratification is physically induced by the buoyancy force of the density gradient in the vertical direction. In this condition, the ability of the exchange and mixing of the momentum between layers is limited. In addition, the turbulent energy dissipates and is no longer able to sustain the sediment particles.

In the following sections, the formulation of the model and concerning boundary conditions are discussed. Then the flow velocity, the suspended sediment concentration, the turbulent kinetic energy, and the dissipation rate for the case of equilibrium flow are discussed for both the cases with and without density stratification effect by including and not including the effect of density stratification. Finally, the linear stability analysis is performed to investigate the bed instability by the effect of density stratification.

2.2 Formulation

2.2.1 Flow equations

The conceptual framework of the problem is an open channel with sufficiently large width to ignore the effect of the bank (Fig. 2-1). The flow is considered to be steady uniform and the bed with constant slope S containing suspended sediment fine enough to assume to follow completely the flow velocity.

Under quasi-steady approximation, the open channel flow can be described by the following two-dimensional Reynolds-averaged Navier-Stokes equations of the form:

$$\tilde{u}\frac{\partial \tilde{u}}{\partial \tilde{x}} + \tilde{w}\frac{\partial \tilde{u}}{\partial \tilde{z}} = \frac{1}{\rho}\left(\frac{\partial \tilde{T}_{xx}}{\partial \tilde{x}} + \frac{\partial \tilde{T}_{xz}}{\partial \tilde{z}}\right) + \mathrm{g}S \tag{2.1}$$

$$\tilde{u}\frac{\partial \tilde{w}}{\partial \tilde{x}} + \tilde{w}\frac{\partial \tilde{w}}{\partial \tilde{z}} = \frac{1}{\rho}\left(\frac{\partial \tilde{T}_{xz}}{\partial \tilde{x}} + \frac{\partial \tilde{T}_{zz}}{\partial \tilde{z}}\right) - \mathrm{g} \tag{2.2}$$

$$\frac{\partial \tilde{u}}{\partial \tilde{x}} + \frac{\partial \tilde{w}}{\partial \tilde{z}} = 0 \tag{2.3}$$

In the above equations, $\tilde{x}$ and $\tilde{z}$ are the coordinates in the streamwise and depth directions, respectively, $\tilde{u}$ and $\tilde{w}$ are the $\tilde{x}$ and $\tilde{z}$ components of velocity, respectively, $\tilde{T}_{xx}$, $\tilde{T}_{xz}$, and $\tilde{T}_{zz}$ are the stress tensors, ρ is the density of fresh water

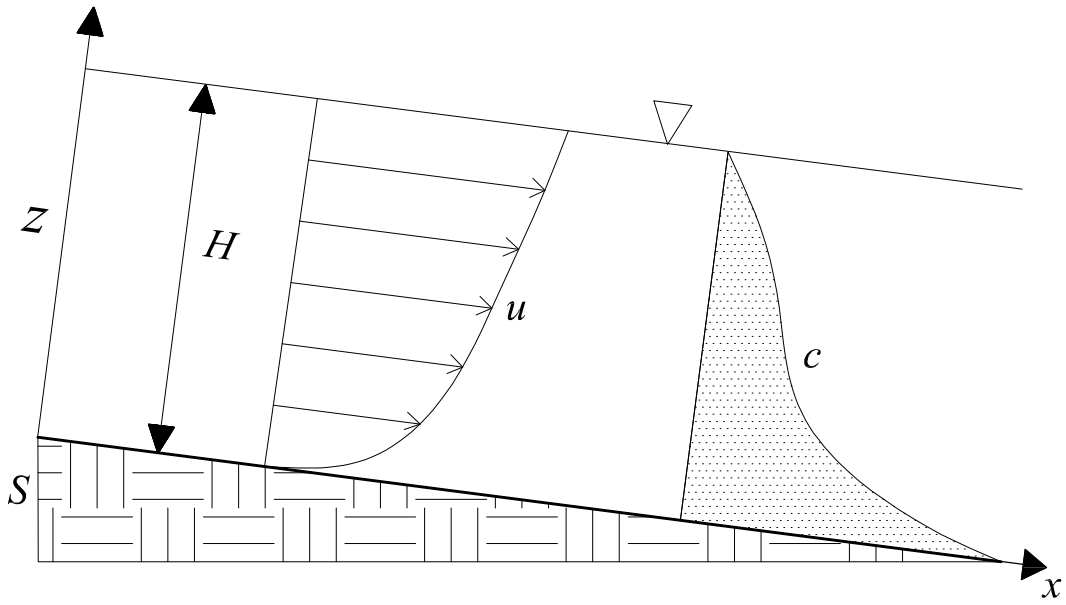

Figure 2-1: Base flow configuration

(= 1000 kg/m^3), g is the acceleration of gravity (= 9.8 m/s^2), and (˜) denotes dimensional variable that is removed to express non-dimensional variables.

The stress tensors are

$$\tilde{T}_{xx} = -\tilde{p} - \overline{\tilde{u}'\tilde{u}'} \tag{2.4}$$

$$\tilde{T}_{xz} = -\overline{\tilde{u}'\tilde{w}'} \tag{2.5}$$

$$\tilde{T}_{zz} = -\tilde{p} - \overline{\tilde{w}'\tilde{w}'} \tag{2.6}$$

where $\tilde{p}$ is the pressure, $-\overline{\tilde{u}'\tilde{u}'}$, $-\overline{\tilde{u}'\tilde{w}'}$, and $-\overline{\tilde{w}'\tilde{w}'}$ are the Reynolds stresses.

The Reynolds stresses are expressed by the use of Boussinesq's kinetmatic eddy viscosity $\tilde{\nu}_t$ such that

$$-\overline{\tilde{u}'\tilde{u}'} = 2\tilde{\nu}_t \frac{\partial \tilde{u}}{\partial \tilde{x}}, \qquad -\overline{\tilde{u}'\tilde{w}'} = \tilde{\nu}_t \left(\frac{\partial \tilde{u}}{\partial \tilde{z}} + \frac{\partial \tilde{w}}{\partial \tilde{x}} \right), \qquad -\overline{\tilde{w}'\tilde{w}'} = 2\tilde{\nu}_t \frac{\partial \tilde{w}}{\partial \tilde{z}} \tag{2.7}$$

where $\tilde{\nu}_t$ is obtained from the turbulent closure models explained later.

2.2.2 Suspended sediment model

The diffusion/dispersion equation of suspended sediment concentration $\tilde{c}$ is

$$\tilde{u} \frac{\partial \tilde{c}}{\partial \tilde{x}} + (\tilde{w} - \tilde{v}_s) \frac{\partial \tilde{c}}{\partial \tilde{z}} = \frac{\partial}{\partial \tilde{x}} \left(-\overline{\tilde{u}'\tilde{c}'} \right) + \frac{\partial}{\partial \tilde{z}} \left(-\overline{\tilde{w}'\tilde{c}'} \right) \tag{2.8}$$

where $\tilde{v}_s$ is the settling velocity of sediment. The turbulent diffusion flux of suspended sediment $-\overline{\tilde{u}'\tilde{c}'}$ and $-\overline{\tilde{w}'\tilde{c}'}$ are expressed by

$$-\overline{\tilde{u}'\tilde{c}'} = \frac{\tilde{\nu}_t}{\sigma_c}\frac{\partial \tilde{c}}{\partial \tilde{x}}, \qquad -\overline{\tilde{w}'\tilde{c}'} = \frac{\tilde{\nu}_t}{\sigma_c}\frac{\partial \tilde{c}}{\partial \tilde{z}} \tag{2.9}$$

where $\sigma_c = 1.2$ is the turbidity Schmidt number for suspended sediment concentration.

The total sediment transport load is assumed to be only the suspended sediment. Therefore, the Exner equation for the sediment mass conservation equation is written in the form

$$-(1-\lambda_p)\frac{\partial \tilde{Z}}{\partial \tilde{t}} = \tilde{E}_s - \tilde{D}_p \tag{2.10}$$

where λ_p is the porosity, $\tilde{Z}$ is the dimensional bed elevation, $\tilde{E}_s$ and $\tilde{D}_p$ are the dimensional entrainment rate of sediment into suspension and the settling rate, respectively, which are written in the form

$$\tilde{E}_s = \tilde{v}_s E_s \tag{2.11}$$

$$\tilde{D}_p = \tilde{v}_s c_b \tag{2.12}$$

where E_s and c_b are the non-dimensional suspended sediment entrainment rate into suspension and the suspended sediment concentration near the bed.

We employ Garcia and Parker [1991] formula to evaluate the suspended sediment entrainment rate of the form

$$E_s = \gamma \frac{A_0 Z_u^5}{1 + \frac{A_0}{0.3} Z_u^5} \tag{2.13}$$

where $A_0 = 1.3 \cdot 10^{-7}$ and γ is an adjustment factor to satisfy the equilibrium condition of the bed in the base state. The non-dimensional parameter Z_u is defined by

$$Z_u = \frac{\tilde{U}_*}{\tilde{v}_s} Re_p^{0.6} \tag{2.14}$$

in which $\tilde{U}_*$, $\tilde{v}_s$, and $Re = \sqrt{R_s g \tilde{d}_s} \tilde{d}_s / \tilde{\nu}$ are shear velocity, settling velocity of sediment and particle Reynolds number, respectively.

2.2.3 k-ϵ model

The standard k-ϵ model includes transport equations for the turbulent kinetic energy k and the turbulent energy dissipation rate ϵ. The kinematic eddy viscosity $\tilde{\nu}_t$ is described by the turbulent energy $\tilde{k}$ and the dissipation rate $\tilde{\epsilon}$ in the form

$$\tilde{\nu}_t = C_\mu \frac{\tilde{k}^2}{\tilde{\epsilon}} \tag{2.15}$$

where the coefficient C_μ is estimated to be 0.09.

The transport equation of turbulent kinetic energy $\tilde{k}$ is

$$\tilde{u} \frac{\partial \tilde{k}}{\partial \tilde{x}} + \tilde{w} \frac{\partial \tilde{k}}{\partial \tilde{z}} = \frac{\partial}{\partial \tilde{x}} \left(\frac{\tilde{\nu}_t}{\sigma_k} \frac{\partial \tilde{k}}{\partial \tilde{x}} \right) + \frac{\partial}{\partial \tilde{z}} \left(\frac{\tilde{\nu}_t}{\sigma_k} \frac{\partial \tilde{k}}{\partial \tilde{z}} \right) + \tilde{P} + \tilde{G} - \tilde{\epsilon} \tag{2.16}$$

where $\sigma_k = 1.0$ is the turbulent Schmidt number for $\tilde{k}$, and $\tilde{P}$ and $\tilde{G}$ are the production due to shear and the production due to buoyancy respectively, described

by

$$\tilde{P} = \tilde{\nu}_t \left[2\left(\frac{\partial \tilde{u}}{\partial \tilde{x}}\right)^2 + \left(\frac{\partial \tilde{u}}{\partial \tilde{z}} + \frac{\partial \tilde{w}}{\partial \tilde{x}}\right)^2 + 2\left(\frac{\partial \tilde{w}}{\partial \tilde{z}}\right)^2 \right] \tag{2.17}$$

$$\tilde{G} = R_s \mathrm{g} \frac{\tilde{\nu}_t}{\sigma_c} \frac{\partial \tilde{c}}{\partial \tilde{z}} \tag{2.18}$$

where R_s is the submerged specific gravity (= 1.65).

The transport equation of the dissipation rate $\tilde{\epsilon}$ is

$$\tilde{u}\frac{\partial \tilde{\epsilon}}{\partial \tilde{x}} + \tilde{w}\frac{\partial \tilde{\epsilon}}{\partial \tilde{z}} = \frac{\partial}{\partial \tilde{x}}\left(\frac{\tilde{\nu}_t}{\sigma_\epsilon}\frac{\partial \tilde{\epsilon}}{\partial \tilde{x}}\right) + \frac{\partial}{\partial \tilde{z}}\left(\frac{\tilde{\nu}_t}{\sigma_\epsilon}\frac{\partial \tilde{\epsilon}}{\partial \tilde{z}}\right) + C_{\epsilon 1}\frac{\tilde{\epsilon}}{\tilde{k}}\left(P + C_{\epsilon 3}G\right) - C_{\epsilon 2}\frac{\tilde{\epsilon}^2}{\tilde{k}} \tag{2.19}$$

where $\sigma_\epsilon = 1.3$ is the turbulent Schmidt number for $\tilde{\epsilon}$, and the parameter $C_{\epsilon 1}$ and $C_{\epsilon 2}$ are 1.44 and 1.92, respectively. The parameter $C_{\epsilon 3}$ is equal to 1 and 0 for the case with and without density stratification effect, respectively.

2.2.4 Mixing length model

With the use of the mixing length turbulent model, the eddy viscosity is expressed by

$$\nu_t = l^2 \left|\frac{\partial u}{\partial z}\right| \tag{2.20}$$

$$l = \kappa(z - Z)\left(\frac{H + R - z}{H}\right)^{1/2} \tag{2.21}$$

where l is mixing length; κ is Karman constant (= 0.4); Z is bed elevation; H is the flow depth; R is the reference level at which the velocity vanishes in the logarithmic velocity distribution.

2.2.5 Normalization

The above governing equation have been normalized by the following normalization:

$$\tilde{t} = \frac{\tilde{H}(1-\lambda_p)}{\tilde{v}_s} t,$$

$$(\tilde{x}, \tilde{z}, \tilde{Z}, \tilde{R}, \tilde{B}) = \tilde{H}(x, z, Z, R, B),$$

$$(\tilde{u}, \tilde{w}) = \tilde{U}_*(u, w), \qquad \tilde{p} = \rho \tilde{U}_*^2 p,$$

$$\tilde{\nu_t} = \tilde{U}_* \tilde{H} \nu_t, \qquad \tilde{c} = \tilde{C} c,$$

$$\tilde{k} = \tilde{U}_*^2 k, \qquad \tilde{\epsilon} = \frac{\tilde{U}_*^3}{\tilde{H}} \epsilon \tag{2.22}$$

Here ($\tilde{}$) denotes the dimensional variables, $\tilde{C}$ is the depth averaged suspended sediment concentration, $\tilde{H}$ is the flow depth, Z, R, and B are the bed elevation, reference level at which the velocity vanishes in the logarithmic velocity distribution, and elevation at which the bed shear stress is evaluated. $\tilde{U}_*$ is the shear velocity described by

$$\tilde{U}_* = \sqrt{\frac{\tilde{\tau}_b}{\rho}} \tag{2.23}$$

where $\tilde{\tau}_b$ is the bed shear stress.

In addition, the depth-averaged suspended sediment concentration $\tilde{C}$ is defined by

$$\tilde{C} = \frac{1}{\tilde{H}} \int_0^{\tilde{H}} \tilde{c} \, d\tilde{z} \tag{2.24}$$

The normalized equations are then take the form

$$u\frac{\partial u}{\partial x} + w\frac{\partial u}{\partial z} = -\frac{\partial p}{\partial x} + \frac{\partial}{\partial x}\left(2\nu_t \frac{\partial u}{\partial x}\right) + \frac{\partial}{\partial z}\left[\nu_t\left(\frac{\partial u}{\partial z} + \frac{\partial w}{\partial x}\right)\right] + 1 \tag{2.25}$$

$$u\frac{\partial w}{\partial x} + w\frac{\partial w}{\partial z} = -\frac{\partial p}{\partial z} + \frac{\partial}{\partial x}\left[\nu_t\left(\frac{\partial u}{\partial z} + \frac{\partial w}{\partial x}\right)\right] + \frac{\partial}{\partial z}\left(2\nu_t \frac{\partial w}{\partial z}\right) - \frac{1}{S} \tag{2.26}$$

$$\frac{\partial u}{\partial x} + \frac{\partial w}{\partial z} = 0 \tag{2.27}$$

$$u\frac{\partial c}{\partial x} + (w - v_s)\frac{\partial c}{\partial z} = \frac{\partial}{\partial x}\left(\frac{\nu_t}{\sigma_c}\frac{\partial c}{\partial x}\right) + \frac{\partial}{\partial z}\left(\frac{\nu_t}{\sigma_c}\frac{\partial c}{\partial z}\right) \tag{2.28}$$

$$\frac{\partial Z}{\partial t} = E_s - c_b \tag{2.29}$$

$$\nu_t = C_\mu \frac{k^2}{\epsilon} \tag{2.30}$$

$$u\frac{\partial k}{\partial x} + w\frac{\partial k}{\partial z} = \frac{\partial}{\partial x}\left(\frac{\nu_t}{\sigma_k}\frac{\partial k}{\partial x}\right) + \frac{\partial}{\partial z}\left(\frac{\nu_t}{\sigma_k}\frac{\partial k}{\partial z}\right) + P + B - \epsilon \tag{2.31}$$

$$u\frac{\partial \epsilon}{\partial x} + w\frac{\partial \epsilon}{\partial z} = \frac{\partial}{\partial x}\left(\frac{\nu_t}{\sigma_\epsilon}\frac{\partial \epsilon}{\partial x}\right) + \frac{\partial}{\partial z}\left(\frac{\nu_t}{\sigma_\epsilon}\frac{\partial \epsilon}{\partial z}\right) + C_{\epsilon 1}\frac{\epsilon}{k}(P + C_{\epsilon 3}B) - C_{\epsilon 2}\frac{\epsilon^2}{k} \tag{2.32}$$

$$P = \nu_t\left[2\left(\frac{\partial u}{\partial x}\right)^2 + \left(\frac{\partial u}{\partial z} + \frac{\partial w}{\partial x}\right)^2 + 2\left(\frac{\partial w}{\partial z}\right)^2\right] \tag{2.33}$$

$$G = Ri_\tau \frac{\nu_t}{\sigma_c}\frac{\partial c}{\partial z} \tag{2.34}$$

where Ri_τ is the shear Richardson number defined with the use of the shear velocity, such that

$$Ri_\tau = \frac{R_s \tilde{C} \mathrm{g} \tilde{H}}{\tilde{U}_*^2} \tag{2.35}$$

2.3 Base state solution

2.3.1 k-ϵ model

Under the equilibrium condition, the derivatives in the streamwise direction x and the vertical component of velocity w can be dropped in the governing equations, which reduce to

$$\frac{\mathrm{d}}{\mathrm{d}z}\left(\nu_t \frac{\mathrm{d}u}{\mathrm{d}z}\right) + 1 = 0 \tag{2.36}$$

$$\frac{\mathrm{d}}{\mathrm{d}z}\left(\frac{\nu_t}{\sigma_c}\frac{\mathrm{d}c}{\mathrm{d}z}\right) + v_s \frac{\mathrm{d}c}{\mathrm{d}z} = 0 \quad \text{or} \quad \frac{\nu_t}{\sigma_c}\frac{\mathrm{d}c}{\mathrm{d}z} + v_s c = 0 \tag{2.37}$$

$$\nu_t = C_\mu \frac{k^2}{\epsilon} \tag{2.38}$$

$$\frac{\mathrm{d}}{\mathrm{d}z}\left(\frac{\nu_t}{\sigma_k}\frac{\mathrm{d}k}{\mathrm{d}z}\right) + \nu_t \left(\frac{\mathrm{d}u}{\mathrm{d}z}\right)^2 + Ri_\tau \frac{\nu_t}{\sigma_c}\frac{\mathrm{d}c}{\mathrm{d}z} - \epsilon = 0 \tag{2.39}$$

$$\frac{\mathrm{d}}{\mathrm{d}z}\left(\frac{\nu_t}{\sigma_\epsilon}\frac{\mathrm{d}\epsilon}{\mathrm{d}z}\right) + C_{\epsilon 1}\frac{\epsilon}{k}\left[\nu_t \left(\frac{\mathrm{d}u}{\mathrm{d}z}\right)^2 + C_{\epsilon 3} Ri_\tau \frac{\nu_t}{\sigma_c}\frac{\mathrm{d}c}{\mathrm{d}z}\right] - C_{\epsilon 2}\frac{\epsilon^2}{k} = 0 \tag{2.40}$$

With the use of Eq. (3.35), Eqs (3.38) and (3.39) are written alternatively in the form

$$\frac{\mathrm{d}}{\mathrm{d}z}\left(\frac{\nu_t}{\sigma_k}\frac{\mathrm{d}k}{\mathrm{d}z}\right) + \nu_t \left(\frac{\mathrm{d}u}{\mathrm{d}z}\right)^2 - Ri_\tau v_s c - \epsilon = 0 \tag{2.41}$$

$$\frac{\mathrm{d}}{\mathrm{d}z}\left(\frac{\nu_t}{\sigma_\epsilon}\frac{\mathrm{d}\epsilon}{\mathrm{d}z}\right) + C_{\epsilon 1}\frac{\epsilon}{k}\left[\nu_t \left(\frac{\mathrm{d}u}{\mathrm{d}z}\right)^2 - C_{\epsilon 3} Ri_\tau v_s c\right] - C_{\epsilon 2}\frac{\epsilon^2}{k} = 0 \tag{2.42}$$

Boundary conditions at the bottom

It is known that, in the thin layer near the bottom (referred to as the bottom layer hereafter), the k-ϵ model cannot reproduce the realistic distributions of flow velocity and suspended sediment concentration very well. We assume that the turbulent structure can be described by the mixing length hypothesis in the bottom

layer. In order to simplify and avoid the singularity due to high gradient at the region near to the bottom, the bottom boundary condition is evaluated at $z = B_0$ which is assumed to be equal to 5% from the bed.

Boundary condition for u

With the use of the mixing length hypothesis, the kinematic eddy viscosity below the bottom layer ($z \leq B_0$) is written in the form

$$\nu_t = \kappa^2 z^2 \left| \frac{\mathrm{d}u}{\mathrm{d}z} \right| \tag{2.43}$$

Substituting the above equation into Eq. (3.34), we obtain

$$\frac{\mathrm{d}}{\mathrm{d}z} \left[\kappa^2 z^2 \left(\frac{\mathrm{d}u}{\mathrm{d}z} \right)^2 \right] = -1 \tag{2.44}$$

Integration of the above equation from the bottom (z=0) to a certain location in the bottom layer (z=z) yields

$$\kappa^2 z^2 \left(\frac{\mathrm{d}u}{\mathrm{d}z} \right)^2 = 1 - z \tag{2.45}$$

where the relation $[\nu_t du/dz]_{z=0} = 1$ has been used. When z is sufficiently small to be ignored, the above equation reduces to

$$\frac{\mathrm{d}u}{\mathrm{d}z} = \frac{1}{\kappa z} \tag{2.46}$$

This is integrated to be

$$u = \frac{1}{\kappa} \ln z + C_0 \tag{2.47}$$

where C_0 is an integral constant to be determined by experimental results. In the case turbulent flow on sufficiently rough walls, it has been known that $C_0 = (1/\kappa)$ $\ln(30/k_s)$, so that Eq. (2.47) reduces to

$$u = \frac{1}{\kappa}\ln\frac{30z}{k_s} \tag{2.48}$$

The above equation is evaluated at the point where $z = B_0$ to become

$$u(B_0) = \frac{1}{\kappa}\ln\frac{30B_0}{k_s} \tag{2.49}$$

This is the boundary condition for velocity where $z = B_0$.

Boundary condition for ϵ

In the vicinity of the bed, we can assume that the production rate is balanced with the dissipation rate, such that

$$\nu_t \left(\frac{\mathrm{d}u}{\mathrm{d}z}\right)^2 = \epsilon \tag{2.50}$$

Substituting Eq. (3.45) into Eq. (3.42) we obtain the relation

$$\nu_t = \kappa z \tag{2.51}$$

with the use of the above equation and Eq. (3.45), Eq. (2.50) is reduced to

$$\epsilon = \frac{1}{\kappa z} \tag{2.52}$$

This equation is evaluated at the outer bound of the bottom layer ($z = B_0$) to be

$$\epsilon(B_0) = \frac{1}{\kappa B_0} \tag{2.53}$$

This is the boundary condition for ϵ where $z = B_0$.

Boundary condition for k

Assuming the continuity of ν_t inside and outside of the bottom layer, we obtain the following equation from Eqs. (3.28) and (2.51)

$$\kappa z = C_\mu \frac{k^2}{\epsilon} \tag{2.54}$$

With the use of Eqs. (2.52) and (2.54), turbulent kinetic energy k is expressed in the relation

$$k(B_0) = \frac{1}{\sqrt{C_\mu}} \tag{2.55}$$

This is the boundary condition for k where $z = B_0$.

Boundary condition for c

The restriction for c can be obtained from the definition of the depth-averaged suspended sediment concentration Eq. (3.22). The normalized form of Eq. (3.22) is

$$\int_0^1 c \, \mathrm{d}z = 1 \tag{2.56}$$

In order to facilitate the problem and to avoid the need to specify the value of suspended sediment concentration c_b explicitly, a new dependent variable is introduced and defined by

$$\chi = \int_0^z c \, \mathrm{d}z \tag{2.57}$$

The boundary condition for χ where $z = B_0$ is written in the form

$$\chi(B_0) = \int_0^{B_0} c \, \mathrm{d}z \tag{2.58}$$

It is assumed $\int_0^{B_0} c \, \mathrm{d}z$ is negligibly small. Dropping the term $\int_0^{B_0} c \, \mathrm{d}z$, the following boundary condition for χ is obtained:

$$\chi(B_0) = 0 \tag{2.59}$$

Boundary conditions at the water surface

At the water surface, the velocity gradient should vanish such that

$$\left.\frac{\mathrm{d}u}{\mathrm{d}z}\right|_{z=1} = 0 \tag{2.60}$$

For the standard k-ϵ model, the turbulent kinetic energy k and the dissipation rate ϵ are assumed to satisfy symmetry conditions. Therefore, the boundary conditions at the free surface $z = 1$ are

$$\left.\frac{\mathrm{d}k}{\mathrm{d}z}\right|_{z=1} = 0 \tag{2.61}$$

$$\left.\frac{\mathrm{d}\epsilon}{\mathrm{d}z}\right|_{z=1} = 0 \tag{2.62}$$

In addition, the boundary condition of χ is

$$\chi(z = 1) = 0 \tag{2.63}$$

Reformulation with the new variable χ

With the use of the new dependent variable χ, Eqs. (3.34), (3.35), (3.40) and (3.41) are expressed by

$$\frac{\mathrm{d}}{\mathrm{d}z}\left(\nu_t \frac{\mathrm{d}u}{\mathrm{d}z}\right) + 1 = 0 \tag{2.64}$$

$$\frac{\nu_t}{\sigma_c}\frac{\mathrm{d}^2\chi}{\mathrm{d}z^2} + v_s\frac{\mathrm{d}\chi}{\mathrm{d}z} = 0 \tag{2.65}$$

$$\nu_t = C_\mu \frac{k^2}{\epsilon} \tag{2.66}$$

$$\frac{\mathrm{d}}{\mathrm{d}z}\left(\frac{\nu_t}{\sigma_k}\frac{\mathrm{d}k}{\mathrm{d}z}\right) + \nu_t\left(\frac{\mathrm{d}u}{\mathrm{d}z}\right)^2 - \mathrm{Ri}_\tau v_s \frac{\mathrm{d}\chi}{\mathrm{d}z} - \epsilon = 0 \tag{2.67}$$

$$\frac{\mathrm{d}}{\mathrm{d}z}\left(\frac{\nu_t}{\sigma_\epsilon}\frac{\mathrm{d}\epsilon}{\mathrm{d}z}\right) + C_{\epsilon 1}\frac{\epsilon}{k}\left[\nu_t\left(\frac{\mathrm{d}u}{\mathrm{d}z}\right)^2 - C_{\epsilon 3}\mathrm{Ri}_\tau v_s\frac{\mathrm{d}\chi}{\mathrm{d}z}\right] - C_{\epsilon 2}\frac{\epsilon^2}{k} = 0 \tag{2.68}$$

The differential system of Eqs. (2.64), (2.65), (2.67), and (2.68) constitute a set of second order differential equations of u, χ, k, and ϵ. Therefore, 8 boundary conditions (Eqs. (2.49), (2.53), (2.55), and (2.59)-(2.63))described in the previous section are required to solve the system.

2.3.2 Mixing model

In mixing length model, we consider logarithmic velocity distribution as the base state condition. To avoid the singularity at the bottom of the bed, variable transformations are introduced in the form

$$\xi = x, \quad \eta = \frac{z - R(x)}{H(x)} \tag{2.69}$$

The logarithmic velocity profile in the base state is described by

$$u_{0,m}(\eta) = \frac{1}{\kappa} ln\left(\frac{\eta + R_0}{R_0}\right) \tag{2.70}$$

where R_0 is the elevation at which the logarithmic velocity is 0 and subscript m refers to the mixing length model.

Here we introduce the concept of friction coefficient C_r which is the ratio between the friction velocity U_* and the depth average velocity U_{avg} of the uniform flow. In addition, this relation also relates the slope S and the Froude number F which is defined by

$$C_r = \frac{U_*}{U_{avg}} = \frac{S^{1/2}}{\mathsf{F}} \tag{2.71}$$

By this definition, integrating Eq. (2.52) from $\eta = 0$ to 1, we obtain

$$\frac{1}{C_r} = \frac{U_{avg}}{U_*} = \frac{1}{\kappa}\left[ln\left(\frac{1+R_0}{R_0}\right) - 1\right] \tag{2.72}$$

where the value $1/C_r = 20$ is adopted [Guy et al., 1966] and the value of R_0 could be determined to be R_0=0.0001234.

The suspended sediment concentration is obtained by solving Eq. (3.8) numerically. In order to compare the result of the mixing length model with that of $k-\epsilon$ model, the boundary condition at the bottom of the suspended sediment is

$$c_{bo,m}(B_0) = c_{bo,k} \tag{2.73}$$

where $c_{bo,m}$ and $c_{bo,k}$ are the normal near bed concentration of mixing length model and $k-\epsilon$ model respectively.

At the water surface, the suspended sediment concentration is zero such that

$$c_{bo,m}(1) = 0 \tag{2.74}$$

2.3.3 Result in steady equilibrium state

It is apparent that the base state problem is not subject to any analytical solutions. The above system of differential equation is solved numerically with the use of the finite volume method.

The results of the numerical calculation are shown in Fig.2-2–2-4. These figures correspond to the vertical distributions of the velocity, the suspended sediment concentration, and the eddy viscosity, respectively. We obtain the results of the case not including the effect of density stratification by solving Eqs. (2.64), (2.65), (2.66), and (2.67) with all the buoyancy terms dropped.

It is found from Fig. 2-2 that the effect of density stratification generally increases the velocity particularly in the upper part and deviates from the logarithmic velocity profile predicted by the mixining length model. In the case of suspended sediment concentration, Fig. 2-3 shows that the effect of density stratification is rather small, and it increases slightly in the lower part and decreases slightly in the upper part due to the effect of density stratification. The concentration is relatively more uniform in the mixing length model. These results can be explained in terms of the eddy viscosity.

The density stratification generally suppresses the turbulent mixing, and therefore, the diffusion of momentum and suspended sediment is reduced. This effect is reflected in Fig. 2-4, which shows that the eddy viscosity decreases due to the density stratification. Because of the reduction of turbulent mixing, relatively large momentum and small suspended sediment concentration in the upper part are not reduced by the effect of small momentum and large sediment concentration near the bed.

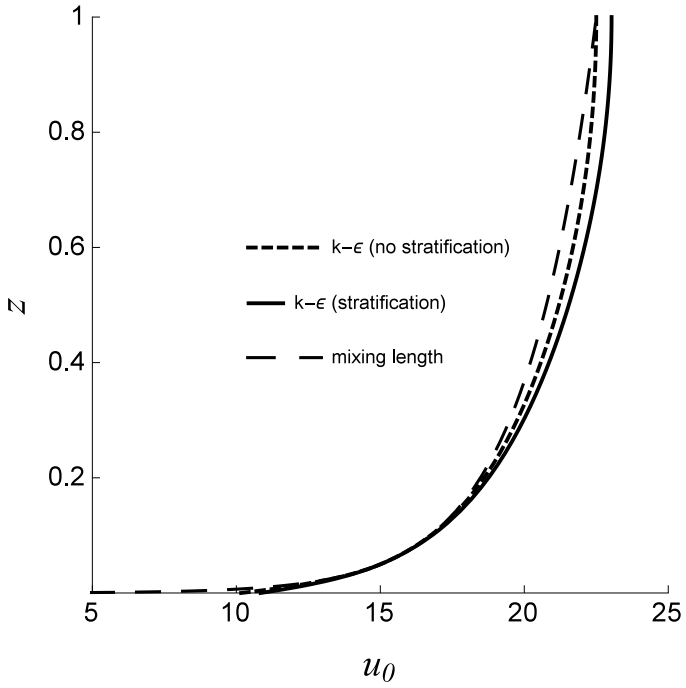

Figure 2-2: Base state flow velocity

2.4 Linear stability analysis

We introduce a coordinate transformation in the form

$$\xi = x \tag{2.75}$$

$$\eta = \frac{z - R(x)}{H(x)} \tag{2.76}$$

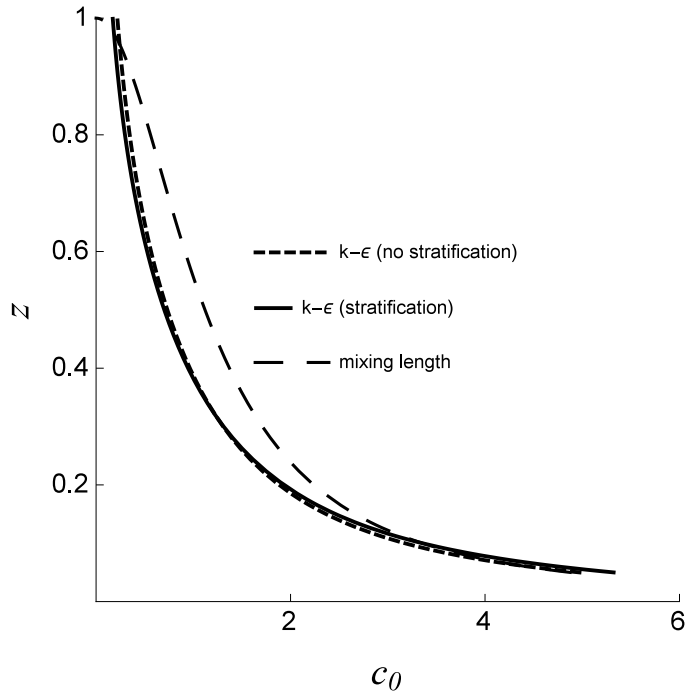

Figure 2-3: Base state concentration

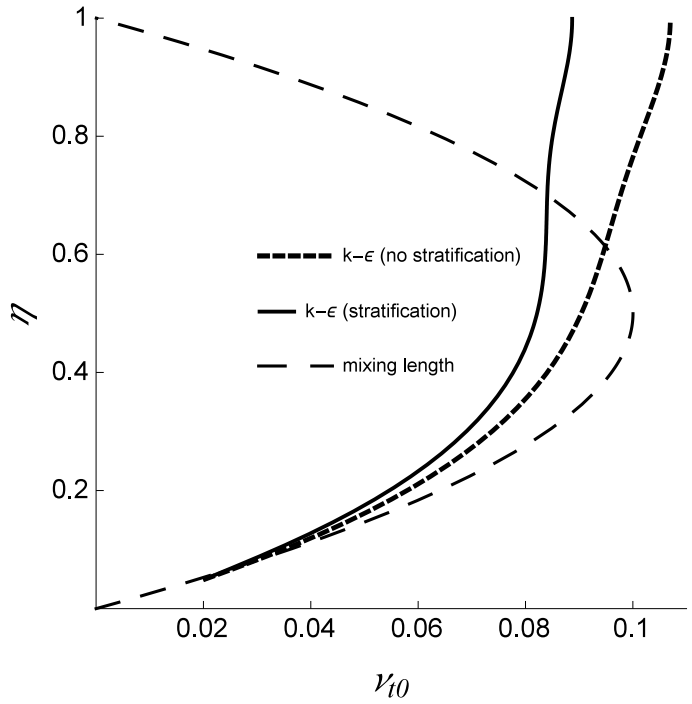

Figure 2-4: Base state eddy viscosity

2.4.1 Perturbation expansion

In the perturbation problem, a small sinusoidal perturbation is imposed on the bed (see Fig.2-5), such that

$$Z = AZ_1 \mathrm{e}^{i(\alpha\xi - \omega t)} \tag{2.77}$$

In response to the perturbation on the bed, all the variables are also perturbed. Because the perturbation has the same wavenumber and complex angular frequency of perturbation, all the variables can be expanded in the form

$$\begin{aligned}(\psi, c, p, k, \epsilon, Z, R, B, H) = (\psi_0, c_0, p_0, k_0, \epsilon_0, 0, R_0, B_0, 1) \\ + A(\psi_1, c_1, p_1, k_1, \epsilon_1, Z_1, Z_1, Z_1, H_1)\mathrm{e}^{i(\alpha\xi - \omega t)}\end{aligned} \tag{2.78}$$

where A, α, and ω are the amplitude, wavenumber, and complex angular frequency of perturbation, respectively. In the above equation, ψ is the stream function defined by

$$u = \frac{\partial \psi}{\partial z} \tag{2.79}$$

$$w = -\frac{\partial \psi}{\partial x} \tag{2.80}$$

2.4.2 General boundary conditions in perturbation problem

The boundary condition at the flat water surface and bed were derived, as discussed in section 2.3. However, it is required to generalize the boundary condition for more general cases such as the perturbed water surface and bed. These boundary conditions are discussed hereafter.

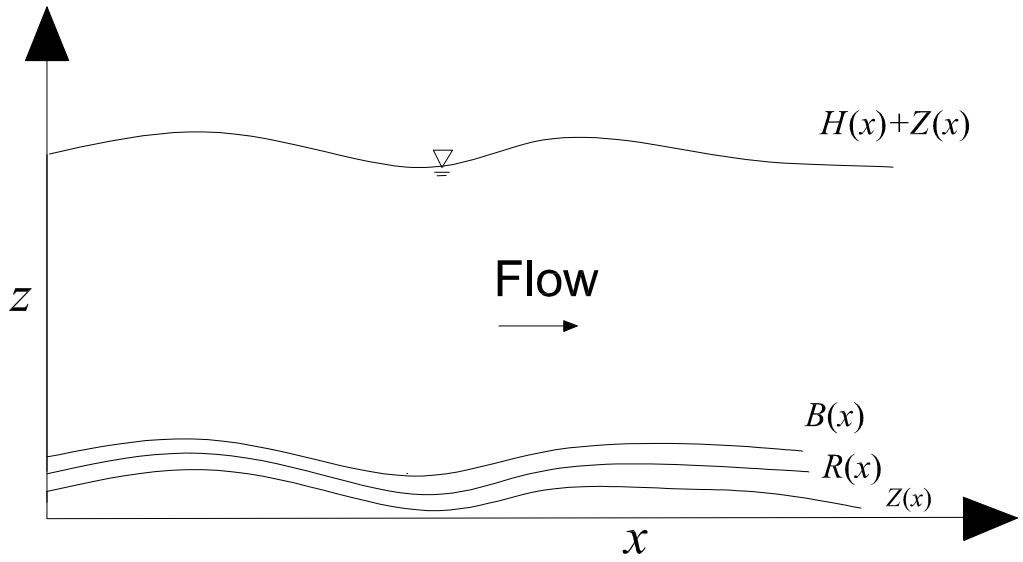

Figure 2-5: Perturbation flow configuration

k-ϵ model

Water surface boundary conditions

At the water surface $\eta = 1$, the stress normal to the water surface should vanish. It is expressed as

$$\vec{e}_{ns} \cdot \ T \cdot \ \vec{e}_{ns} = 0 \tag{2.81}$$

where $\vec{e_{ns}}$ is the unit vector normal to the water surface and T is the stress tensor.

The kinematic boundary condition that th velocity component normal to the water surface vanishes is expressed as

$$\vec{u} \cdot \vec{e}_{ns} = 0 \tag{2.82}$$

In addition, the diffusion flux of the turbulent kinetic energy and dissipation normal to the water surface also vanish, such that

$$\vec{F_k} \cdot \vec{e}_{ns} = 0 \tag{2.83}$$

$$\vec{F_\epsilon} \cdot \vec{e}_{ns} = 0 \tag{2.84}$$

where $\vec{F_k}$ and $\vec{F_\epsilon}$ are the diffusion flux of the turbulent kinetic k and the dissipation rate ϵ, defined by

$$\vec{F_k} = (-\frac{\nu_t}{\sigma_k}\frac{\partial k}{\xi}, -\frac{\nu_t}{\sigma_k}\frac{\partial k}{\partial \eta}) \tag{2.85}$$

$$\vec{F_\epsilon} = (-\frac{\nu_t}{\sigma_\epsilon}\frac{\partial \epsilon}{\xi}, -\frac{\nu_t}{\sigma_\epsilon}\frac{\partial \epsilon}{\partial \eta}) \tag{2.86}$$

The suspended sediment flux across the water surface also vanish

$$(\vec{F_c} - v_s c(\xi, 1)\vec{k}) \cdot \vec{e}_{ns} = 0 \tag{2.87}$$

where $\vec{k} = (0, 1)$ is normal unit vector, $\vec{F_c}$ is the suspended sediment flux, defined as

$$\vec{F_c} = (-\frac{\nu_t}{\sigma_c}\frac{\partial c}{\partial \xi}, -\frac{\nu_t}{\sigma_c}\frac{\partial c}{\partial \eta}) \tag{2.88}$$

Bottom boundary conditions

The bottom boundary condition is evaluated at $\eta_b = 0.05$ from the bed.

The boundary conditions of the normal and tangential velocity component are

$$\vec{u} \cdot \vec{\mathrm{e}}_{nb} = 0 \tag{2.89}$$

$$\vec{u} \cdot \vec{\mathrm{e}}_{tb} - \frac{1}{\kappa}\ln\frac{30\eta_b}{k_s} = 0 \tag{2.90}$$

where $\vec{\mathrm{e}}_{nb}$ and $\vec{\mathrm{e}}_{tb}$ are the normal and tangential unit vector to the bottom layer.

The eddy viscosity should be continuous inside and outside of the bottom layer η_b

$$\kappa^2\eta_b^2\frac{\partial u}{\partial \eta} = C_\mu\frac{k(\xi, \eta_b)^2}{\epsilon(\xi, \eta_b)} \tag{2.91}$$

In addition, we assume that the production rate due to shear is balanced with the dissipation at the bottom

$$P = \epsilon(\xi, \eta_b) \tag{2.92}$$

Furthermore, the suspended sediment flux is equal to the entrainment rate of suspended sediment into suspension from the bottom, such that

$$\vec{F_c} \cdot \vec{\mathrm{e}}_{nb} = E_s(U_*) \tag{2.93}$$

Mixing length model

In mixing length model, the boundary condition for the suspended sediment is the same as those in the k-ϵ model. However, the vanishing bottom tangential and normal velocity components are applied at the reference level R.

$$\vec{u} \cdot \vec{e}_{nr} = 0 \tag{2.94}$$

$$\vec{u} \cdot \vec{e}_{tr} = 0 \tag{2.95}$$

where $\vec{e}_{nr}$ and $\vec{e}_{tr}$ are the unit vector normal and tangential to R.

2.4.3 Solution of perturbation problem

In the scheme of linear stability analysis, the amplitude A is assumed to be infinitesimally small and higher non-linear terms of A are negligible. The wavenumber α is real number, and the angular frequency of perturbation ($\omega = \omega_r + i\omega_i$) is complex number. The real and imaginary parts of ω are the real angular frequency and the growth rate of perturbation, respectively.

Substituting Eq. (2.78) into the governing equations, we obtain the perturbation equations. Since the amplitude of the perturbation A is considered to be infinitesimally small, the terms associated with higher non-linear order of $\mathcal{O}(A^2)$ are negligible.

The perturbation equations cannot be solved analytically; therefore, some numerical scheme has to be introduced.The spectral collocation method incorporated with the Chebyshev polynomials are used to solved the perturbation equations.

k-ϵ model

The variables ψ_1, c_1, k_1, and ϵ_1 are expanded in the form

$$\psi_1 = \sum_{j=0}^{N} a_j T_j(\zeta) \tag{2.96}$$

$$c_1 = \sum_{j=0}^{N} a_{(N+1)+j} T_j(\zeta) \tag{2.97}$$

$$k_1 = \sum_{j=0}^{N} a_{(2N+2)+j} T_j(\zeta) \tag{2.98}$$

$$\epsilon_1 = \sum_{j=0}^{N} a_{(3N+3)+j} T_j(\zeta) \tag{2.99}$$

where $a_j (j = 0, 1, \ldots, 4N + 3)$ are the coefficients of the Chebyshev polynomials, and $T_j(\zeta)$ is the Chebyshev polynomials of degree j. The independent variable ζ ranges from -1 to 1 and relates to the physical coordinate $\eta (B_0 < \eta < 1)$ by

$$\zeta = 2 \frac{\ln(\frac{\eta - R_0}{B_0 - R_0})}{\ln(\frac{1 - R_0}{B_0 - R_0})} \tag{2.100}$$

The Eqs. (2.96), (2.97) , (2.98), and (2.99) are substituted into the perturbation equations evaluated at the Gauss-Lobatto points ζ_n, described by

$$\zeta_n = \cos\left(\frac{n\pi}{N}\right) \tag{2.101}$$

where $n = 0, 1, ..., N$. In addition, the perturbation variable H_1 is assigned as a_{4N+4}. We eventually obtain a system of $4N + 5$ algebraic equations, ten of which are replaced by the boundary conditions. Extracting all the unknow coefficient $a_j (j = 0, 1, ..., 4N + 4)$, we obtain a system of algebraic equations, written in the

matrix form

$$\mathbb{L} \cdot [a_0 \ a_1 \ a_2 \ ... \ a_{4N+4}]^T = \mathbb{M} \cdot Z_1 \tag{2.102}$$

where $\mathbb{L}$ is a $(4N+5) \times (4N+5)$ matrix the elements of which are the coefficient of the perturbed variables ψ_1, c_1, k_1, ϵ_1, and H_1 of the perturbation equations and of the boundary conditions, and $\mathbb{M}$ is a vector with $(4N+5)$ elements, which are the coefficient of Z_1. By solving Eq. (2.102), we obtain the solutions for perturbed variables ψ_1, c_1, k_1, ϵ_1, and H_1. Substituting these solutions into the Exner equation (3.27), we obtain the complex angular frequency of perturbation ω.

Mixing length model

Similarly, the perturbed stream function $\psi_{1,m}$, concentration $c_{1,m}$, and depth $H_{1,m}$ of the mixing length model also adopt a numerical scheme, spectral collocation method. The variables are expanded as follow

$$\begin{aligned} &\psi_{1,m} = \sum_{j=0}^{N} a_{j,m} T_{j,m}(\zeta_m), \quad c_{1,m} = \sum_{j=0}^{N} a_{(N+1)+j,m} T_{j,m}(\zeta_m) \\ &H_{1,m} = a_{2N+2} \end{aligned} \tag{2.103}$$

where ζ_m is related to $\eta (0 < \eta < 1)$ and defined by

$$\zeta_m = 2\eta - 1 \tag{2.104}$$

The similar procedures to the $k - \epsilon$ model are then proceeded. We eventually obtain the system of algebraic equations for the mixing length model in the matrix form

$$\mathbb{K} \cdot [a_{0,m} \ a_{1,m} \ ... \ a_{2N+2,m}]^T = \mathbb{N} \cdot Z_1 \tag{2.105}$$

where $\mathbb{K}$ is a $(2N+3) \times (2N+3)$ matrix the elements of which are the coefficient

of the perturbed variables $\psi_{1,m}$, $c_{1,m}$, and $H_{1,m}$ of the perturbation equations and of the boundary conditions, and $\mathbb{N}$ is the $(2N+3)\times 1$ matrix the elements of which are the coefficient of perturbed variable R_1 of the mixing length model.

2.5 Results and discussion

2.5.1 Characteristics of bed instability

One example of the results of stability analysis is shown in Fig.2-6. In the figure, the solid line is the neutral curve where the growth rate of perturbation vanishes ($\omega_i = 0$). The bed is unstable when the growth rate is positive ($\omega_i > 0$) and stable when the growth rate is negative ($\omega_i < 0$). The dashed line is the neutral curve of the real part of the angular frequency of perturbation ($\omega_r = 0$) which is associated with the celerity of the bedwaves. The bedwaves migrate downstream and upstream when ω_r is are positive and negative, respectively.

According to Fig.2-6, an unstable region, bounded by solid line, is observed in the upper flow regime Froude number $F > 1$). The unstable region corresponds to the formation of the antidunes. The experimental results of Kennedy [1961] are also plotted in the figure. It is found that the results predicted by the model agree fairly well with the experimental results.

2.5.2 Migration direction of antidunes

In the unstable region, the dashed line divides the region into two parts. On the left side of the dashed line, the celerity is negative ($\omega_r < 0$), indicating that the antidunes are migrating in the upstream direction. On the other hand, on the right

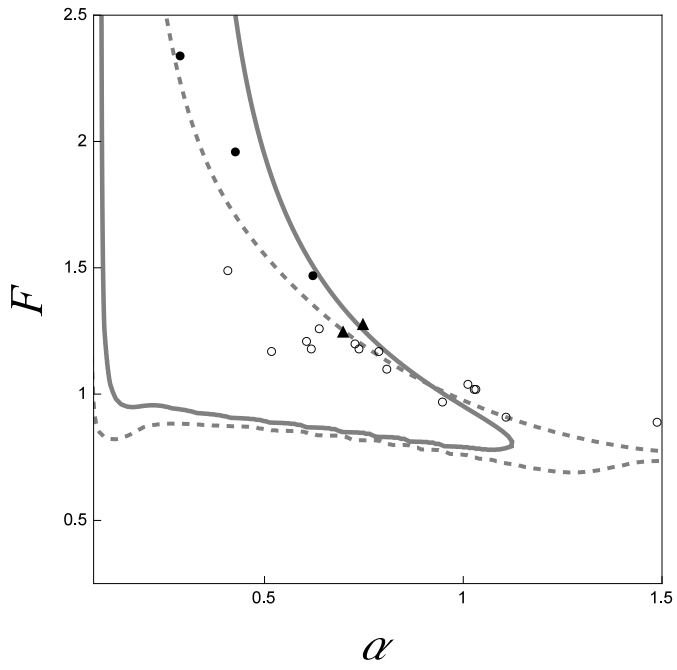

Figure 2-6: Stability diagram. Kennedy's experiment: •, d_m=0.549mm upstream migration antidune; ▲, d_m=0.549mm downstream migration antidune; ○, d_m=0.233mm upstream migration antidune.

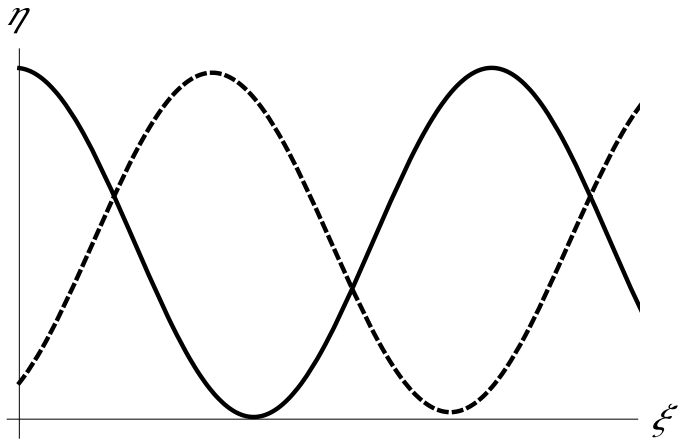

Figure 2-7: Upstream migrating antidunes (F=1.5, α=0.4).Bed elevation(solid line), net erosion(dashed line)

side of the dashed line, ω_r is positive, indicating that the antidunes are migrating in the downstream direction.

Among Kennedy's experimental data, two downstream migrating antidunes are observed. Compared with the other upstream migrating antidunes for the same experimental condition, it is observed that the downstream migrating antidunes are those with shorter wavelength. The current model is qualitatively consistent with the experimental result on the migration direction of the antidunes.

In order to discuss the mechanism of instability and the migration direction of antidunes, we focus on the bed elevation and the net erosion rate ($E_s - c_b$) of two typical cases: one is upstream-migrating antidunes shown in Fig.2-7, and the other is downstream-migrating antidunes shown in Fig.2-8. In the figures, the solid lines correspond to the bed elevation, while the dashed line corresponds to the net erosion rate.

Fig.2-7 shows the bed elevation and the net erosion rate in the case that $F = 1.5$

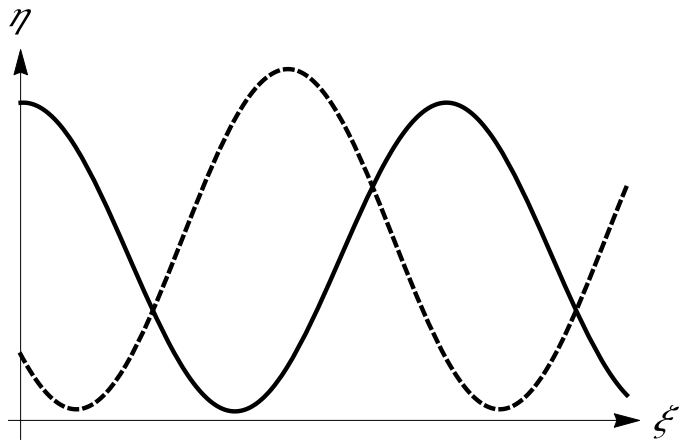

Figure 2-8: Downstream migrating antidue (F=1.5, α=0.6). Bed elevation (solid line), net erosion(dashed line)

and $\alpha = 0.4$, corresponding to upstream-migrating antidunes. According to Fig.2-7, the net erosion rate is out of phase with the bed elevation. The net erosion rate is largest near the trough of the bed wave, and smallest near the crest. This indicates that the erosion occurs at the trough, while the deposition occurs at the crest. By this process, the amplitude of the bed wave increases. In addition, there is a lag between the maximum erosion (deposition) and the trough (crest) of the bed. The maximum erosion and deposition occurs at the location slightly upstream of the trough and the crest of the bed wave, respectively. This signifies that the bed wave is moving in the upstream direction.

Fig.2-8 shows the case $F = 1.5$ and $\alpha = 0.6$, corresponding to downstream-migrating antidunes. The bed elevation and the net erosion rate are out of phase again, and therefore, the flat bed is unstable. In this case, however, the maximum erosion and deposition take place at the location slightly downstream of the trough and the crest of the bed wave (see Fig.2-8). Therefore, the bed wave migrates in the downstream direction.

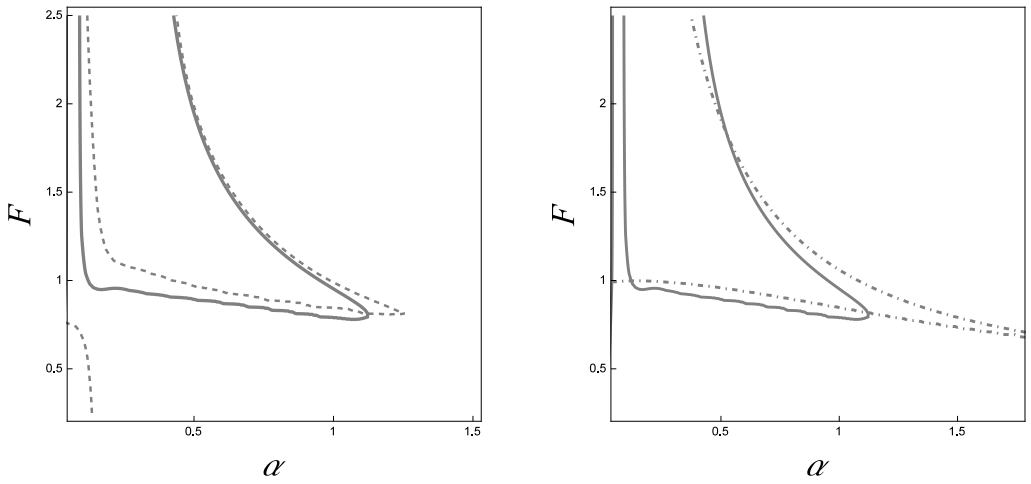

(a) (b)

Figure 2-9: Instability diagram: (a) k-ϵ model: solid line, with density stratification; dashed line, without density stratification; (b): solid line, k-ϵ model; dot-dashed line, mixing length model

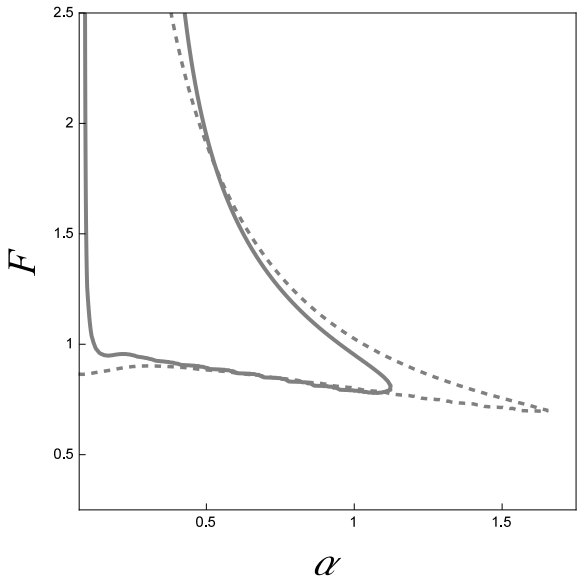

Figure 2-10: Stability diagram of k-ϵ model $v_s = 0.2$(solid line) and $v_s = 0.1$(dashed line)

2.5.3 Density stratification effect

The effect of density stratification on the bed instability is studied by comparing the results of linear stability analysis including and not including the effect of density stratification by k-ϵ model (see Fig.2-9(a)). The condition without the effect of density stratification is obtained by ignoring all the terms associated with suspended sediment concentration gradient. In addition, the comparison of the result of k-ϵ model and that of mixing length model is shown in Fig.2-9(b).

The neutral curves of the growth rate of perturbation ω_i are shown in Fig.2-9. The solid line is the neutral curve with the effect of density stratification while the dashed line is that without the effect of density stratification, and the dot-dashed line is the result of mixing length model. As seen in Fig.2-9(a), the unstable region decreases to lower critical Froude number (minimum Froude number in the unstable region) due to the effect of density stratification. In addition, the unstable region in the range of large wavenumbers in the vicinity of the critical Froude number disappears when the effect of density stratification is included. According to Fig.2-9(b), the result by mixing length model not including the density stratification effect is consistent with the case without density stratification effect by k-ϵ such that the critical Froude number is higher and the instability expands towards the range of bigger wavenumbers.

In addition, we investigate the effect of the parameter settling velocity v_s to the stability of the bed. The stability diagram of the analysis for the cases $v_s = 0.2$ and $v_s = 0.1$ are shown in Fig.2-10. In this figure, the solid line and dashed line are the neutral curve of the growth rate of perturbation for the cases $v_s = 0.2$ and $v_s = 0.1$, respectively. Smaller settling velocity corresponds to the less stratified condition. According to the figure, the unstable region expands in the direction of

larger wavenumbers in the vicinity of critical Froude number for the case of smaller settling velocity $v_s = 0.1$.

2.6 Conclusion

In this study, we performed linear stability analysis with the concept of varying eddy viscosity by the mixing length model and the standard k-ϵ model. In the latter model, the effect of density stratification due to suspended sediment is investigated.

The Reynolds-averaged Navier-Stokes equations and dispersion/diffusion equation of suspended sediment coupled with the turbulent closure of both the mixing length model and k-ϵ are found to be capable of predicting the bed instability. The unstable region predicted by the analysis is in fairly good agreement with the experimental results. The formation of antidunes is observed in the upper flow regime. The model explains physical process of instability and the migration direction of the antidunes.

In k-ϵ model, the transport equations of turbulent kinetic energy and the dissipation rate include the buoyancy term to study the effect of density stratification . In the base state, the effect of density stratification increases the flow velocity, and decreases the suspended sediment concentration in the upper part and increases near the bed. These results are caused by the general decrease in the eddy viscosity due to the suppression of turbulent mixing by the density stratification.

In linear stability analysis, an unstable region appears at the upper flow regime which corresponds to the formation of the antidunes when only suspended load is considered. The model is in fair agreement with the experimental results. In

addition, the model reveals the migration mechanism of the antidunes in both upstream and downstream directions. The long wavelength antidunes usually migrate in the upstream direction, whereas shorter wavelength antidunes migrate in the downstream direction. Moreover, it is found that the effect of density stratification decreases the critical Froude number. In addition, density stratification stabilizes the bed in the range of large wavenumbers in the vicinity of the critical Froude number.

Notation

The following symbols are used:

A	= amplitude of perturbation (–)
A_0	= constant $1.3 \cdot 10^{-7}$ (–)
a_j	= Chebyshev polynomial coefficient (–)
B	= elevation of top of bedload layer (–)
C	= non-dimensional depth averaged concentration (–)
C_0	= integral constant (–)
$C_{\epsilon 1}, C_{\epsilon 2}, C_{\epsilon 3}, C_\mu$	= k-ϵ model constants (–)
c	= non-dimensional suspended sediment concentration (–)
c_b	= non-dimensional near bed concentration(–)
c'	= turbulent concentration fluctuation (–)
d_s	= sediment diameter (mm)
D_g	= gradient sediment diameter (mm)
E_s	= entrainment rate into suspension (–)
$\vec{e}_{ns}, \vec{e}_{nb}$	= unit vector normal to surface and bed (–)
$\vec{e}_{ts}, \vec{e}_{tb}$	= unit vector tangent to surface and bed (–)
F	= Froude number (–)

$\vec{F_c}$ = suspended sediment flux (–)

$\vec{F_k}$ = turbulent energy flux (–)

$\vec{F_\epsilon}$ = dissipation rate diffusion flux (–)

G = production of turbulent energy by buoyancy

g = gravity acceleration (ms^{-2})

H = non-dimensional flow depth (–)

i = imaginary number (–)

k = non-dimensional turbulent kinetic energy (–)

k_s = bed roughness (–)

l = mixing length (–)

$\mathbb{K}$, $\mathbb{L}$, $\mathbb{M}$, $\mathbb{N}$ = matrix (–)

P = non-dimensional production of turbulent energy due to shear (–)

p = non-dimensional pressure (–)

R = elevation of reference level (–)

R_s = submerged specific gravitiy (–)

Re_p = particle Reynold number (–)

S = slope (–)

Ri_τ = shear Richarson number (–)

$T, T_{xx}, T_{xz}, T_{zz}$ = shear stress (–)

T_j = Chebyshev polynomial (–)

t = non-dimensional time (–)

U_{avg} = average velocity (–)

U_* = non-dimensional shear velocity (–)

u = non-dimensional streamwise velocity (–)

u' = turbulent streamwise velocity fluctuation (–)

$\vec{u}$ = velocity vector (–)

v_s = non-dimensional particle settling velocity (–)

w = non-dimensional vertical velocity (–)

w' = turbulent vertical velocity fluctuation (–)

x = streamwise coordinate (–)

Z = bed elevation (–)

Z_u = entrainment rate relation parameter (–)

Z_1 = perturbation function (–)

z = vertical coordinate (–)

α = wavenumber (–)

γ = adjusting coefficient (–)

ϵ = dissipation rate (–)

ζ = independent variables of Chebyshev polynomial(–)

κ = Karman constant (–)

λ_p = porosity (–)

ν_t = non-dimensional eddy viscosity (–)

ξ = transformed streamwise coordinate (–)

ρ = water density (kg.m^{-3})

$\sigma_c, \sigma_k, \sigma_\epsilon$ = Schmidt number of suspended sediment, kinetic energy, and dissipation ra

τ_b = bed shear stress(–)

χ = accumulated suspended sediment(–)

ψ = stream function (–)

$\omega, \omega_i, \omega_r$ = complex frequency, growthrate, and celerity of perturbation (–)

$(\tilde{\ })$ = dimensional quantity scaled by $\tilde{H}$ and $\tilde{U}_*$ (–)

Chapter 3

Bed instability generated by turbidity current

3.1 Introduction

Turbidity current is generated once fine sediment is entrained into the flow on the ocean floor and flows in the downslope direction. This kind of current is sustained by the force exerting on the excess suspended sediment in the flow. Due to its high capability to erode the bed and transport the sediment, it is considered as one of the major mechanisms that shape and form submarine morphology, i.e. subaqueous canyon and gullies. In addition, the turbidity currents transport not only the sediment but also the turbidite with rich hydrocarbon matters which are the most important source of petroleum and methane hydrate. However, the turbidity currents also possess destructive power on the environments through which they flow. Reaching the speeds of 20 m/s (Piper et al. [1999]), the turbidity currents are capable of destroying and breaking submarine network cable.

In this study, we propose a linear stability analysis of bed waves formed due to instability between the ocean floor and turbidity currents with the use of the

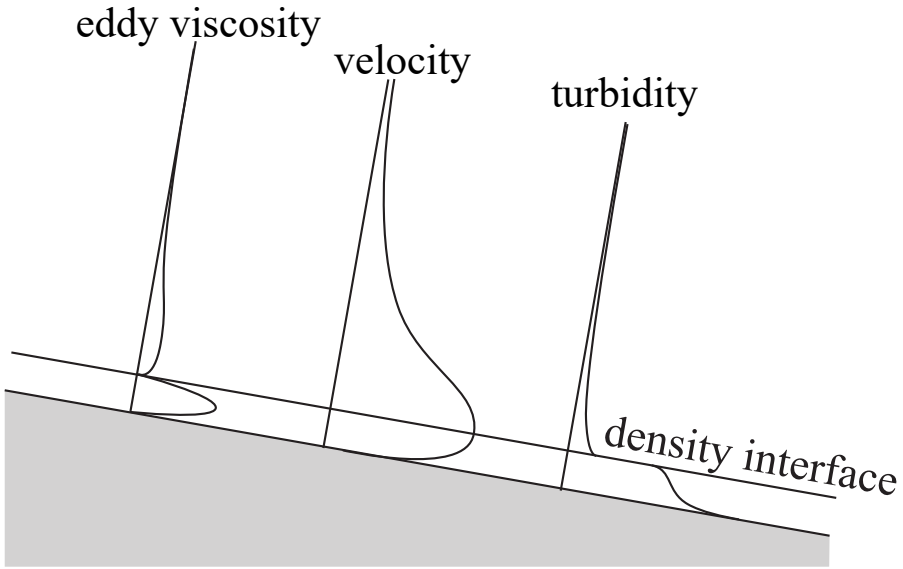

Figure 3-1: Conceptual flow of turbidity current in normal state condition

assumption of normal flow condition and a simple turbulent model, the mixing length hypothesis. In the analysis, we employ the flow equations including the concentration of suspended sediment as the driving force, the dispersion/diffusion equation of suspended sediment, and the continuity equation describing the time variation of the bed elevation. Normalizing those governing equations, we obtain two important non-dimensional parameters: the densimetric Froude number and the settling velocity.

3.2 Equilibrium condition of turbidity currents

Considering a saline or thermal density plume flows down an incline plane, the high salt concentration or temperature plume will increase its thickness as it flows downstream. During the increase of thickness, the plume reduces its concentration. Without any external energy supplied to the plume, it cannot move travel distance.

Luchi et al. [2015] adopted the concept similar to turbidity current with the roof (Cantero et al. [2009]). However, a flux-free surface is imposed as upper boundary instead of a rigid roof. They employed standard k-ϵ model to investigate the flow velocity and suspended sediment concentration distribution of the turbidity current. With the assumption of flux-free boundary, the turbidity current does not entrain ambient fluid from the upper boundary. Thus, the turbidity current might possess an equilibrium solution under this consideration. In order to investigate the effect of the upper boundary, a numerical simulation is performed under the condition of increasing the height of the upper flux-free boundary. It is found that an equilibrium state exists at the vicinity of the bottom layer in which the suspended concentration is very high. This equilibrium layer is found to be independent from the increase of height of the upper layer.

Fig.3-1 shows a conceptual diagram of turbidity current. The flow velocity becomes zero at the bottom and upper boundary. In line with this, there exists a location at which the velocity gradient becomes zero. In this vicinity, the turbulence intensity decreases while the eddy viscosity and turbulent diffusion flux also decrease.

At the density interface where the velocity gradient is zero, the turbulent diffusion flux vanishes and the density gradient of suspended sediment goes to infinity. In this context, the suspended sediment concentration decreases abruptly at the density interface (Fig. 3-1). The region from the bed to the density interface is called "driving layer" , and the region above the density interface is called "driven layer" . It is found that the thickness of the driving layer at equilibrium condition is invariant (Luchi et al. [2015]).

In the driven layer, the suspended sediment concentration does not necessarily

become zero, however, the profile is subject to similarity solution. By using k-ϵ turbulence model, Fukushima and Hayakawa [1990] found that the plume in the inclined plane possesses similarity solution. The flow velocity near the bottom is constant, while the concentration decreases as the plume flows downstream. In addition, the thickness of the plume is also increasing. The similarity solution is also applied to the turbidity currents. The concentration is discontinuous at the density interface. At the lower part of the driven layer, the velocity is constant while the concentration decreases. Comparing with the driving layer, the concentration in the outer layer is negligibly small.

The shear stress vanishes at the interface between the high concentration driving layer and driven layer. In other words, the forces that govern the flow of the driving layer is, indeed, the gravity force within the layer and the shear stress generated at the bottom. Therefore, the flow in the driving layer is independent from the driven layer. Within the driving layer, the normal condition is satisfied when the gravity force is balanced with the bed shear stress. This condition is equivalent to normal flow condition in an open channel flow. Under this consideration, the turbidity current is expected to be able to flow continuously as long as the suspended sediment concentration is maintained.

3.3 Formulation

3.3.1 Flow equation

The turbidity currents (see Fig.3-2) are described by two-dimensional Reynolds-averaged Navier-Stokes equation with the use of Boussinesq approximation as well

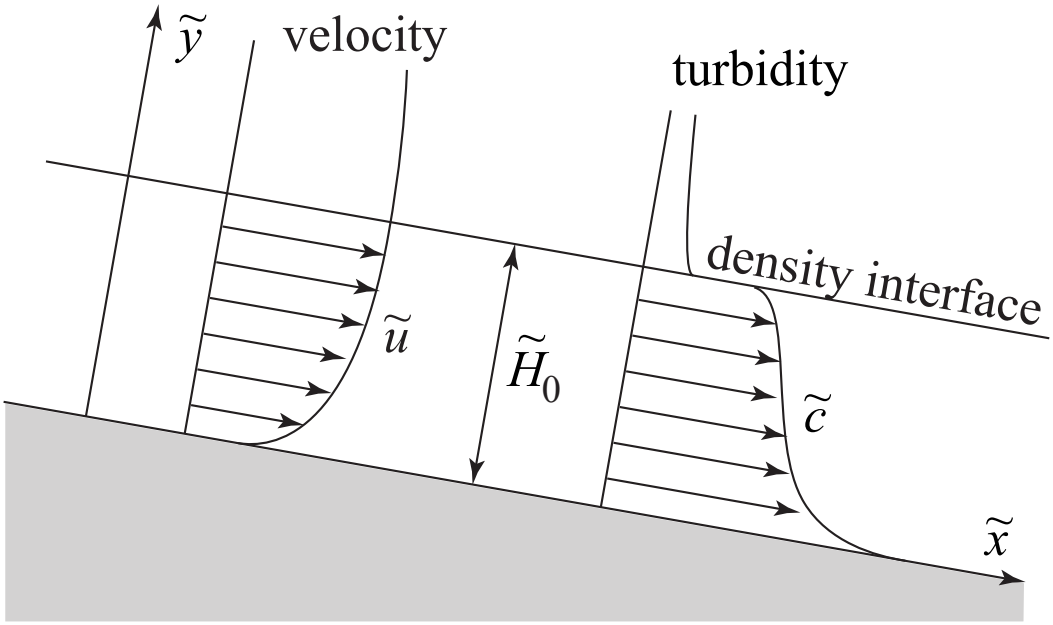

Figure 3-2: Coordinate and conceptual diagram of the high concentration lower layer

as the continuity equation, defined as

$$\tilde{u}\frac{\partial \tilde{u}}{\partial \tilde{x}} + \tilde{v}\frac{\partial \tilde{u}}{\partial \tilde{y}} = \frac{1}{\rho}\left(\frac{\partial \tilde{T}_{xx}}{\partial \tilde{x}} + \frac{\partial \tilde{T}_{xy}}{\partial \tilde{y}}\right) + (1 + R_s\tilde{c})\, gS \tag{3.1}$$

$$\tilde{u}\frac{\partial \tilde{v}}{\partial \tilde{x}} + \tilde{v}\frac{\partial \tilde{v}}{\partial \tilde{y}} = \frac{1}{\rho}\left(\frac{\partial \tilde{T}_{xy}}{\partial \tilde{x}} + \frac{\partial \tilde{T}_{yy}}{\partial \tilde{y}}\right) - (1 + R_s\tilde{c})\, g \tag{3.2}$$

$$\frac{\partial \tilde{u}}{\partial \tilde{x}} + \frac{\partial \tilde{v}}{\partial \tilde{y}} = 0 \tag{3.3}$$

where $\tilde{x}$ and $\tilde{y}$ are the streamwise and depth directions, $\tilde{u}$ and $\tilde{v}$ are the velocity component in $\tilde{x}$ and $\tilde{y}$ directions, respectively, $\tilde{T}_{ij}(i, j = x, y)$ is the stress tensor, ρ is the density of seawater, g is the acceleration of gravity, R_s is the submerged specific weight of the sediment, $\tilde{c}$ is the suspended sediment concentration, and S is the slope of the ocean floor. The $(\tilde{})$ denotes the dimensional quantity which will be non-dimensionalized later.

The stress tensor is evaluated by the use of mixing length model, described by

$$\tilde{T}_{ij} = -\tilde{p}\delta_{ij} + \rho\tilde{\nu}_t \left(\frac{\partial \tilde{u}_j}{\partial \tilde{x}_i} + \frac{\partial \tilde{u}_i}{\partial \tilde{x}_j} \right) \tag{3.4}$$

$$\tilde{\nu}_t = \tilde{l}^2 \left| \frac{\partial \tilde{u}}{\partial \tilde{y}} \right|, \quad \tilde{l} = \kappa \left(\tilde{y} - \tilde{Z} \right) \left(\frac{\tilde{H} + \tilde{R} - \tilde{y}}{\tilde{H}} \right)^{1/2} \tag{3.5}$$

where $\tilde{p}$ is the pressure, $\tilde{\nu}_t$ is the eddy viscosity, κ is the Karman constant ($= 0.4$), $\tilde{H}$ is the thickness of the high density layer, Z is the bed elevation, and R is the reference level at which logarithmic velocity distribution becomes zero.

3.3.2 Sediment transport equation

The suspended sediment is considered to be sufficiently small that follows completely the flow except its settling velocity $\tilde{v}_s$ in the vertical direction. The settling velocity is the parameter which induces the self-stratification in the turbidity current. In addition, the hindered settling effect is also neglected. The dispersion/diffusion equation of the suspended sediment concentration is

$$\frac{\partial \tilde{u}\tilde{c}}{\partial \tilde{x}} + \frac{\partial \left(\tilde{v} - \tilde{v}_s \right) \tilde{c}}{\partial \tilde{y}} = \frac{\partial}{\partial \tilde{x}} \left(\tilde{\nu}_t \frac{\partial \tilde{c}}{\partial \tilde{x}} \right) + \frac{\partial}{\partial \tilde{y}} \left(\tilde{\nu}_t \frac{\partial \tilde{c}}{\partial \tilde{y}} \right) \tag{3.6}$$

It is the settling velocity $\tilde{v}_s$, an important parameter, that limit the thickening of the equilibrium layer and induce the self stratification of the turbidity current.

3.3.3 Normalization

The above governing equations have been normalized as follows

$$\left(\tilde{x}, \tilde{y}, \tilde{H}, \tilde{Z}, \tilde{R} \right) = \tilde{H}_0 \left(x, y, H, Z, R \right)$$

$$(\tilde{u}, \tilde{v}, \tilde{v}_s) = \tilde{U}_{f0}\,(u, v, v_s)$$

$$\left(\tilde{p}^*, \tilde{T}_{ij}\right) = \rho \tilde{U}_{f0}^2\,(p, T_{ij})$$

$$\tilde{c} = \tilde{C} c \tag{3.7}$$

where $\tilde{U}_f$ is the friction velocity, the subscribe 0 denotes the quantity in the base state condition, $\tilde{p}^*$ is the piezometric pressure, $\tilde{C}$ is the depth-averaged suspended sediment concentration. The piezometric pressure $\tilde{p}^*$ and the depth-averaged suspended sediment concentration $\tilde{C}$ are defined by

$$\tilde{p}^* = \tilde{p} + \rho g\,(S\tilde{x} - \tilde{y}) \tag{3.8}$$

$$\tilde{C} = \frac{1}{\tilde{H}_0} \int_0^{\tilde{H}_0} \tilde{c} \mathrm{d}\tilde{z} \tag{3.9}$$

Therefore, the governing equations (3.1)-(3.6) become

$$u\frac{\partial u}{\partial x} + v\frac{\partial u}{\partial y} = \left(\frac{\partial T_{xx}}{\partial x} + \frac{\partial T_{xy}}{\partial y}\right) + c \tag{3.10}$$

$$u\frac{\partial v}{\partial x} + v\frac{\partial v}{\partial y} = \left(\frac{\partial T_{xy}}{\partial x} + \frac{\partial T_{yy}}{\partial y}\right) - R_{i\tau} c \tag{3.11}$$

$$\frac{\partial u}{\partial x} + \frac{\partial v}{\partial y} = 0 \tag{3.12}$$

$$T_{ij} = -p\delta_{ij} + \rho\nu_t \left(\frac{\partial u_j}{\partial x_i} + \frac{\partial u_i}{\partial x_j}\right) \tag{3.13}$$

$$\nu_t = l^2 \left|\frac{\partial u}{\partial y}\right|, \quad l = \kappa\,(y - Z)\left(\frac{H + R - y}{H}\right)^{1/2} \tag{3.14}$$

$$\frac{\partial uc}{\partial x} + \frac{\partial\,(v - v_s)\,c}{\partial y} = \frac{\partial}{\partial x}\left(\nu_t \frac{\partial c}{\partial x}\right) + \frac{\partial}{\partial y}\left(\nu_t \frac{\partial c}{\partial y}\right) \tag{3.15}$$

where $R_{i\tau}$ is the shear Richardson number, defined by

$$R_{i\tau} = \frac{gS\tilde{C}\tilde{H}_0}{\tilde{U}_{f0}^2} \tag{3.16}$$

3.4 Base state solution

In order to facilitate the application of the boundary conditions at the bottom and upper boundary, we introduce the coordinate transformation

$$(\xi, \eta) = \left(x, \frac{y - R(x)}{H(x)} \right) \tag{3.17}$$

where R is the reference level at which the velocity is 0 in the logarithmic velocity distribution. The mixing length l then becomes

$$l = \kappa H \left(\eta + \frac{R - Z}{H} \right) (1 - \eta)^{1/2} \tag{3.18}$$

In the above equation, the term $(R - Z)/H \ll 1$ is negligibly small.

In the base state condition, the streamwise derivative and the vertical component of velocity are 0 and can be dropped from the governing equations. Thus, Eqs (3.10) and (3.15) are simplified to

$$\frac{\mathrm{d}}{\mathrm{d}\eta} \left[\kappa^2 \eta^2 (1 - \eta) \left(\frac{\mathrm{d}u_0}{\mathrm{d}\eta} \right)^2 \right] + c_0 = 0 \tag{3.19}$$

$$\kappa^2 \eta^2 (1 - \eta) \frac{\mathrm{d}u_0}{\mathrm{d}\eta} \frac{\mathrm{d}c_0}{\mathrm{d}\eta} + v_s c_0 = 0 \tag{3.20}$$

where the subscribe 0 denotes the solution in the base state condition.

The boundary conditions of the flow are vanishing velocity at the bottom and zero gradient at the upper boundary

$$u(\eta = 0) = 0, \qquad \left.\frac{\mathrm{d}u}{\mathrm{d}\eta}\right|_{\eta=1} = 0 \tag{3.21}$$

The new dependent variable $\chi = \int_0^z c$ is introduced in order to facilitate the application of the boundary conditions. We obtain the boundary conditions of χ defined as

$$\chi(\eta = 0) = 0, \qquad \chi(\eta = 1) = 1 \tag{3.22}$$

In order to solve Eqs (3.19) and(3.20), a numerical method is required. Here, we employ finite volume method to solve for the solutions of the base state condition.

In the governing equations of the base state solution, we have a dimensionless settling velocity parameter $v_s (= \tilde{v}_s / \tilde{U}_{f0})$. The effects of the settling velocity on the flow velocity and the suspended sediment concentration of the turbidity currents are then discussed herein. The flow velocity and suspended sediment concentration profile for various values of v_s are shown in Fig.3-3 and Fig. 3-4, respectively. For the same friction velocity $\tilde{U}_{f0}$, smaller settling velocity represents a smaller sediment size.

According to Fig. 3-4, the suspended sediment is almost uniform in the depth direction when the settling velocity is very small ($v_s = 0.01$), and the flow velocity becomes larger particularly in the upper part (Fig. 3-3). Due to the tendency of the sediment particles to settle down, the suspended sediment concentration profile deviates from the uniform profile under the condition of increasing settling velocity, and it is found that the suspended sediment concentration increases in the region near to the bottom and decreases in the upper part.

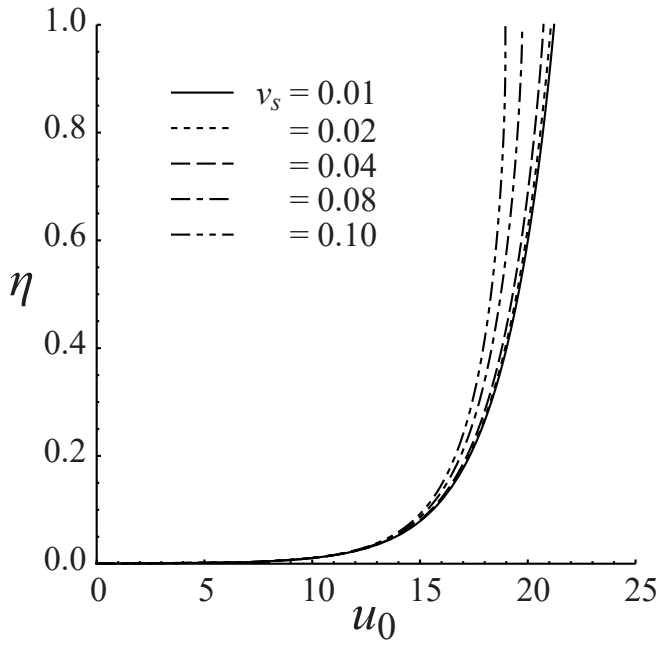

Figure 3-3: Flow velocity profile in the base state condition

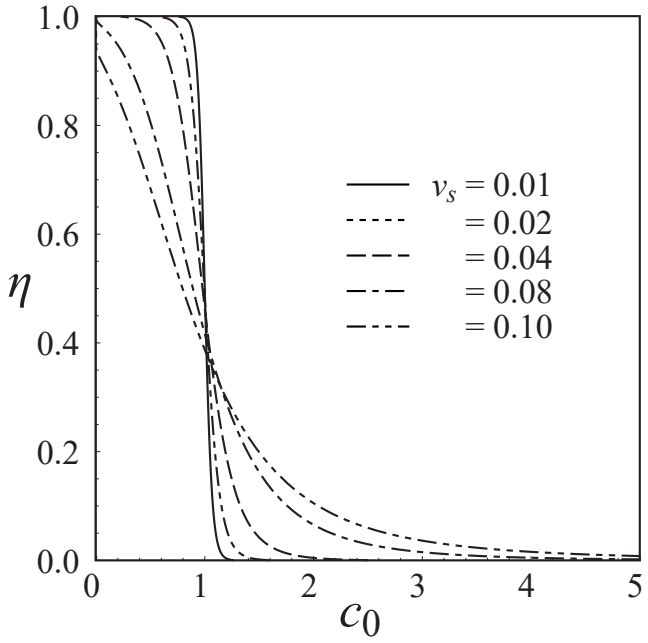

Figure 3-4: Suspended sediment concentration profile in the base state condition

In addition, when the settling velocity v_s is bigger than 0.08, the suspended sediment concentration at the density interface becomes 0. This implies that the assumption that there exists a density interface no longer holds when $v_s > 0.08$. Therefore, it is suggested that the turbidity current does not possess equilibrium conditions for the case when v_s is larger than 0.08.

3.5 Linear stability analysis

3.5.1 Perturbation expansion

In the perturbation problem, we impose a small disturbance to the base state condition in the form

$$(\psi, c, p, H, Z, R) = (\psi_0, c_0, P_0, 1, 0, R_0) + A\,(\psi_1, c_1, P_1, H_1, R_1, R_1) \exp\left[\mathrm{i}\,(k\xi - \omega t)\right] \quad (3.23)$$

where A, k, and ω are the amplitude of perturbation, wavenumber, and angular frequency of perturbation, respectively. In linear theory, the amplitude A is assumed to be infinitesimally small. The wavenumber k is real number, whereas angular frequency of perturbation $\omega = \omega_r + i\omega_i$ is complex number. In addition, ψ is the stream function.

Substituting the perturbation variables into the governing equation Eqs.(3.10)-(3.15), we obtain the perturbation equations at the order of A, defined as

$$\mathcal{L}(\eta)^c c_1(\eta) + \mathcal{L}^{\psi}(\eta)\,\psi_1(\eta) + \mathcal{L}^{H}(\eta)\,H_1 = 0 \quad (3.24)$$

$$\mathcal{R}^{\psi}(1)\ \psi_1(\eta) + \mathcal{R}^{H}(1)\ H_1 = 0 \tag{3.25}$$

$$\mathcal{M}^{c}(\eta)c_1(\eta) + \mathcal{M}^{\psi}(\eta)\psi_1(\eta) + \mathcal{M}^{H}(\eta)H_1 = 0 \tag{3.26}$$

$$\psi_1(1) = \psi_1(0) = \mathcal{D}\psi_1(0) = 0 \tag{3.27}$$

where $\mathcal{L}^{\phi}$,$\mathcal{R}^{\phi}$, and $\mathcal{M}^{\phi}$ ($\phi = c, \psi, H$) are the linear differential operators of the perturbation variables, the detail expressions of which are too complicated and long to include here. The operator $\mathcal{D} = \mathrm{d}/\mathrm{d}\eta$ is the derivative with respect to the depth direction.

3.5.2 Boundary conditions of the perturbation problem

At the density interface, the normal velocity component, the normal stress, and normal sediment flux are zero, defined by

$$\boldsymbol{u} \cdot \boldsymbol{e}_{ns} = 0 \quad \text{at} \quad \eta = 1 \tag{3.28}$$

$$\boldsymbol{e}_{ns} \cdot \boldsymbol{T} \cdot \boldsymbol{e}_{ns} = 0 \quad \text{at} \quad \eta = 1 \tag{3.29}$$

$$\boldsymbol{F}_s \cdot \boldsymbol{e}_{ns} - v_s c\, \boldsymbol{k} \cdot \boldsymbol{e}_{ns} = 0 \quad \text{at} \quad \eta = 1 \tag{3.30}$$

where $\boldsymbol{u}$ is the velocity vector ($= (u, v)$), $\boldsymbol{F}_s$ is the suspended sediment flux vector ($= (-\nu_t \partial c/\partial x, -\nu_t \partial c/\partial y)$), $\boldsymbol{k}$ is normal unit vector ($= (0, 1)$), $\boldsymbol{e}_{ns}$ is the unit vector normal to the density interface, and $\boldsymbol{T}$ is the stress tensor defined by

$$\boldsymbol{T} = \begin{bmatrix} T_{xx} & T_{xy} \\ T_{xy} & T_{yy} \end{bmatrix} \tag{3.31}$$

At the bottom, the normal and tangential velocity component are zero

$$\boldsymbol{u} \cdot \boldsymbol{e}_{nb} = 0 \quad \text{at} \quad \eta = 0 \tag{3.32}$$

$$\boldsymbol{u} \cdot \boldsymbol{e}_{tb} = 0 \quad \text{at} \quad \eta = 0 \tag{3.33}$$

where $\boldsymbol{e}_{nb}$ and $\boldsymbol{e}_{tb}$ are the unit vector normal and tangential to the bed.

The sediment flux at the bottom is equal to the entrainment rate of suspended sediment into suspension $\mathcal{E}_s$.

$$\boldsymbol{F}_s \cdot \boldsymbol{e}_{nb} - \mathcal{E}_s = 0 \quad \text{at} \quad \eta = 0.05 \tag{3.34}$$

3.5.3 Solution of perturbation problem

A numerical method is used to solve the perturbation problem as it is not subject to any analytical solutions. In this study, we employ the spectral collocation method with the Chebyshev polynomials. The perturbation variable ψ_1 and c_1 are expanded in the form

$$\psi_1 = \sum_{n=0}^{N} a_n T_n(\zeta) \tag{3.35}$$

$$c_1 = \sum_{n=N+1}^{2N+1} a_n T_n(\zeta) \tag{3.36}$$

where T_n is the Chebyshev polynomials of degree n, $\zeta[-1, 1]$ is an independent variable, defined by

$$\zeta = 2 \left\{ \frac{\ln[(\eta + R_0)/R_0]}{\ln[(1 + R_0)/R_0]} \right\} - 1 \tag{3.37}$$

Substituting Eqs (3.34) and (3.35) into the perturbation equations evaluated at Gauss-Lobatto point

$$\zeta_j = \cos(j\pi/N), \quad (j = 1, \cdots, N-2) \tag{3.38}$$

We obtain a system of $(2N+3) \times (2N+3)$ algebraic equations, six of which are the boundary conditions. Extracting all the unknown coefficient a_n, the equations

can be written in matrix form

$$\mathbb{L}\boldsymbol{a} = \boldsymbol{b}R_1 \tag{3.39}$$

where $\mathbb{L}$ is a $(2N+3)\times(2N+3)$ matrix the elements of which are the coefficients of the perturbed variables ψ_1, c_1, and H_1 of the perturbation equations and boundary conditions, $\boldsymbol{a}[a_0, a_1, ..., a_{2N+2}, H_1]^T$, and $\boldsymbol{b}$ is a vector with $(2N+3)$ elements. The solution vector $\boldsymbol{a}$ is

$$\boldsymbol{a} = \mathbb{L}^{-1}\boldsymbol{b}R_1 \tag{3.40}$$

From the above result, we can determine the solution of the perturbation variables ψ_1, c_1, and H_1.

As far as the turbidity current is concerned, the suspended sediment is assumed to be dominant, whereas the bedload is negligible. The temporal variation of the bed elevation can be described by the Exner equation in the form

$$\frac{\partial Z}{\partial t} = \mathcal{D}_s - \mathcal{E}_s \tag{3.41}$$

where $\mathcal{D}_s$ and $\mathcal{E}_s$ are the settling flux and the entrainment rate of suspended sediment into suspension, respectively. We can determine the settling flux and the entrainment rate by

$$\mathcal{D}_s = \beta c_a, \quad \mathcal{E} = u_f^{\gamma} \tag{3.42}$$

where $\beta = \tilde{v}_s\tilde{C}/\tilde{\mathcal{E}}_0$, c_a is the suspended sediment concentration evaluated at $\eta = 0.05$ from the bed, the entrainment rate is proportional to the friction velocity u_f to the power $\gamma = 5$ in this formulation.

The Exner equation (3.41) is expanded and manipulated to obtain the equation

at order A

$$-\omega R_1 = c_1 - \mathcal{E}_\psi \psi_1 \tag{3.43}$$

The complex angular frequency of perturbation are then obtained in the form

$$\omega = -(c_1 - \mathcal{E}_\psi \psi_1)/R_1 = f\left(k, R_{i\tau}, v_s\right) \tag{3.44}$$

The imaginary part ω_i is the growth rate of the perturbation. The bed is stable when $\omega_i < 0$, whereas the bed is unstable when $\omega_i > 0$.

3.6 Results and discussion

We now proceed to the discussion of the results of the analysis. Fig.3-5 shows the neutral curve of ω_i obtain from the analysis. Fig. 3-5 (a), (b), (c), and (d) correspond to the result of the cases which settling velocity $v_s = 0.01$, 0.02, 0.04, and 0.08, respectively. The horizontal axis is the wavenumber k, and the vertical axis is the densimetric Froude number F. The density Froude number F relates to the shear Richardson number by

$$F^2 = C_f / R_{i\tau} \tag{3.45}$$

where C_f is the friction coefficient and it is assumed to be $C_f = 1/400$ in this analysis.

According to Fig.3-5 , the instability of the flat bed occurs at the value of densimetric Froude number approximately bigger than 0.4. At the vicinity of the critical Froude number region, the instability wavenumber is in the range of (1-1.5). As the F increases, the range of instability wavenumber reduces approximately to the range of (0.1-1.0).

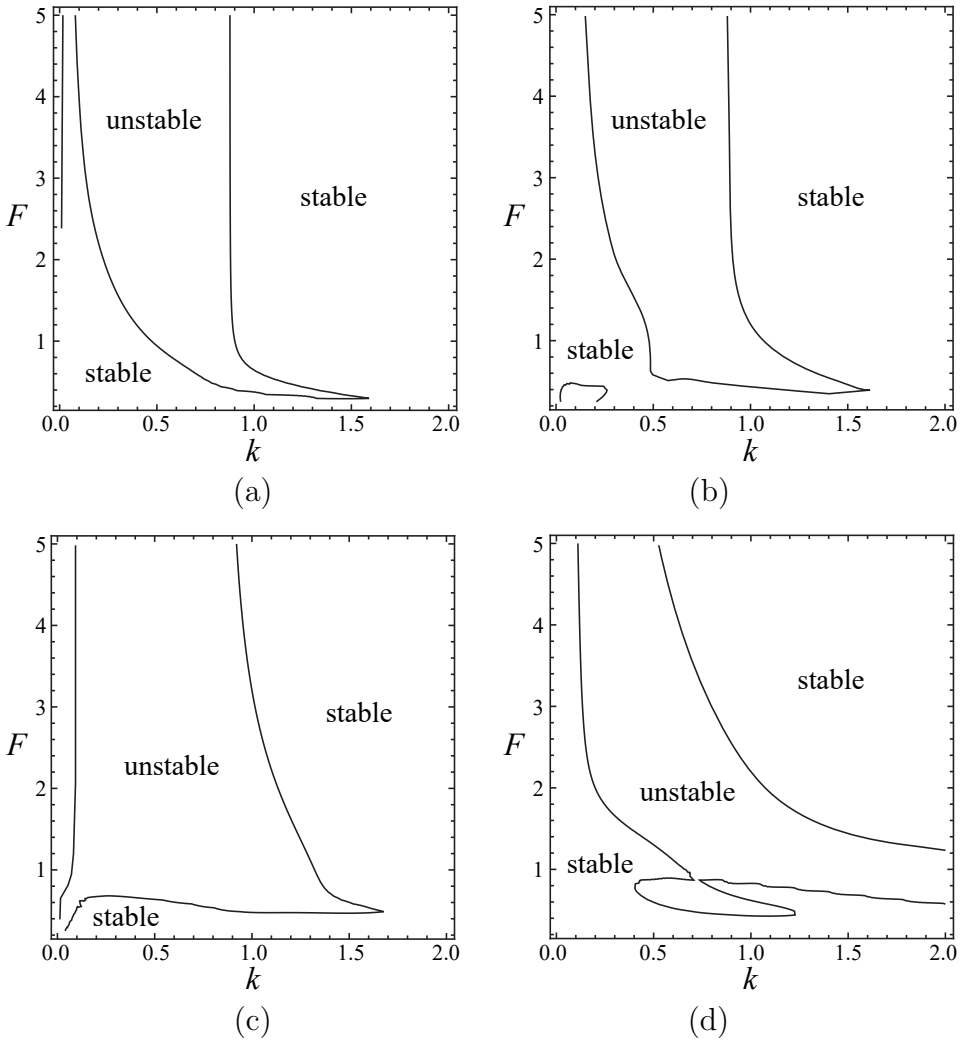

Figure 3-5: Bed instability diagram generated by turbidity current (a) $v_s = 0.01$, (b) $v_s = 0.02$, (c) $v_s = 0.04$, (d) $v_s = 0.08$.

In addition, as mentioned before, turbidity currents do not seem to possess any normal flow condition if the settling velocity v_s is greater than 0.08. According to Fig.3-5(d), it is found that the shape of the instability region is strange and without any physical implications.

Fig.3-6 shows the instability diagram in open channel flow condition. We obtain the results by removing the term c from the momentum equations (3.10) and (3.11). Fig.3-6(a) and (b) corresponds to the cases which v_s=0.01 and 0.04, respectively. According to Fig.3-6(a), we can see that the result of the unstable region resembles that of the turbidity current when the settling velocity $v_s = 0.01$. As we can see from the normal flow condition, the driving force generated by the suspended sediment is almost uniform in the depth direction. However, in the case of settling velocity $v_s = 0.04$, the instability region of open channel is different from that of turbidity current because of the decrease of suspended sediment at the density interface.

3.7 Conclusion

The turbidity currents possesses equilibrium condition at least at the layer near to the bottom which is independent from the upper diluted layer. In this context, we perform linear stability analysis to investigate the instability of the bed generated by the turbidity current.

In the base state condition, the decrease of the settling velocity increases the suspended sediment concentration at the density interface. As the driving force is generated by the suspended sediment increases, the flow velocity at the density interface also increases.

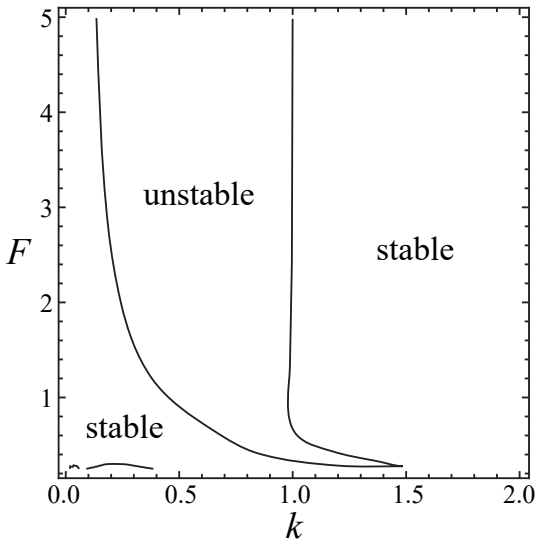

(a)

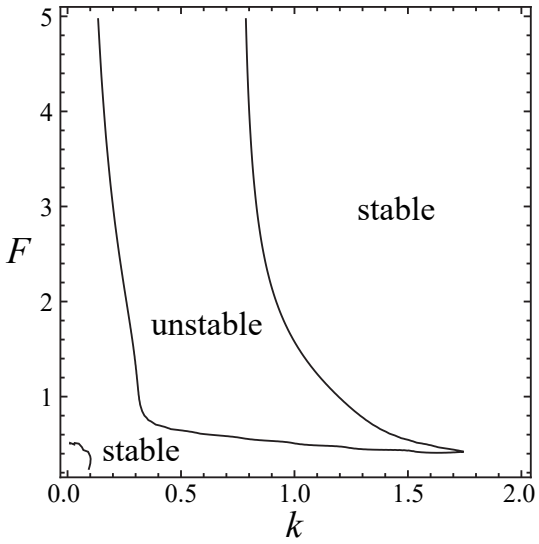

(b)

Figure 3-6: Instability diagram in open channel. (a) $v_s = 0.01$, (b) $v_s = 0.04$

However, in the equilibrium state, the suspended sediment decrease to zero at the density interface as the settling velocity is greater than 0.08. This result is physically impossible. In line with this, it is suggested that equilibrium state of the turbidity currents does not exist in the case of large sediment particle.

According to the results of the stability analysis, the plane bed becomes unstable when the densimetric Froude number is greater than 0.4. In addition, at the vicinity of the critical Froude number, the wavenumber of the unstable bed is in the range of 1.0-1.5, whereas when Froude number increases, the range of unstable wavenumber reduces to the range of 0.1-1.0.

Comparing the instability diagrams of the turbidity current and open channel flow when in the range of small settling velocity ($v_s = 0.01$), it is found that the unstable region of the two cases are very similar. It is convenient to explain the similarity of these results from the perspective of the driving force of the flow. Gravity force is acting on the water in open channel flow, and acting on suspended sediment in the turbidity current. While the driving force is almost uniform in the depth direction when the suspended sediment is small for the two flow configurations, it is therefore reasonable to obtain the similar results.

Notation

The following symbols are used:

A	= amplitude of perturbation (–)
a_n	= Chebyshev polynomial coefficient (–)
$\boldsymbol{a}$, $\boldsymbol{b}$	= vector

C = non-dimensional depth averaged concentration (–)

C_0 = integral constant (–)

c = non-dimensional suspended sediment concentration (–)

c_a = non-dimensional near bed concentration(–)

$\mathcal{D}$ = derivative operator(–)

$\mathcal{D}_s$ = deposition rate (–)

$\mathcal{E}_s$ = entrainment rate into suspension (–)

$\boldsymbol{e}_{ns}$,$\boldsymbol{e}_{nr}$, $\boldsymbol{e}_{nb}$ = unit vector normal to surface, reference level, and bed (–)

$\boldsymbol{e}_{ts}$,$\boldsymbol{e}_{tr}$, $\boldsymbol{e}_{tb}$ = unit vector tangent to surface, reference level, and bed (–)

F = Froude number (–)

$\boldsymbol{F}_s$ = suspended sediment flux (–)

g = gravity acceleration (ms^{-2})

H_0 = flow depth at base state condition (–)

i = imaginary number (–)

k = wavenumber (–)

l = mixing length (–)

$\mathcal{L},\ \mathcal{M},\ \mathcal{R}$ = linear operator of perturbation variables (–)

$\mathbb{L}$ = matrix (–)

p = non-dimensional pressure (–)

R = elevation of reference level (–)

R_s = submerged specific gravitiy (–)

Ri_τ = shear Richarson number (–)

S = slope (–)

$T, T_{xx}, T_{xy}, T_{yy}$ = shear stress (–)

T_n = Chebyshev polynomials (–)

t = non-dimensional time (–)

U_{f0} = shear velocity at base state condition (–)

u = non-dimensional streamwise velocity (–)

$\boldsymbol{u}$ = velocity vector (–)

v = non-dimensional vertical velocity (–)

v_s = non-dimensional particle settling velocity (–)

x = streamwise coordinate (–)

y = vertical coordinate (–)

Z = bed elevation (–)

γ = constant (–)

ζ = independent variables of Chebyshev polynomial(–)

κ = Karman constant (–)

ν_t = non-dimensional eddy viscosity (–)

ξ = transformed streamwise coordinate (–)

ρ = water density (kg.m^{-3})

χ = accumulated suspended sediment(–)

ψ = stream function (–)

$\omega, \omega_i, \omega_r$ = complex frequency, growthrate, and celerity of perturbation (–)

$(\tilde{\ })$ = dimensional quantity scaled by $\tilde{H}_0$ and $\tilde{U}_{f0}$ (–)

subscript $(\ )_0$ = denote the base state(–)

subscript $(\ )_1$ = denote the base state(–)

Chapter 4

Conclusions

In this study, we perform linear stability analysis in two configurations (open channel flow and turbidity current) of suspended sediment dominated environments. As long as the suspended sediment is concerned, density stratification affects the flow velocity distribution, suspended sediment concentration, the turbulent kinetic energy, and its dissipation rate. In addition, density stratification is expected to have influence on the formation of the bedwaves of the open channel and turbidity current.

In open channel flow, the sediment transport is assumed to be solely suspended sediment. This condition corresponds to the upper regime flow and relatively fine sediment. In order to investigate the effect of density stratification on the vertical flow structures, we employ the standard k-ϵ model as the turbulent closure. The turbulent model includes the production due to buoyancy term in the transport equations of turbulent kinetic energy and its dissipation rate. The buoyancy term involves with the gradient of suspended sediment concentration which represents the effect of density stratification By removing the terms associated with buoyancy, we obtain the case without density stratification.

The results from Chapter 2 shows that density stratification increases the flow velocity at the upper part of the flow. It is also found that the suspended sediment concentration slightly increases at the bottom and decreases at the upper part. These results can be explained in terms of the turbulent mixing capacity. The density stratification generated by the gradient of the suspended sediment generally suppresses the turbulent mixing. As the result, the diffusion of momentum and suspended sediment is restrained. This is reflected by the reduce of the eddy viscosity in the case with density stratification effect included.

It is also found that the standard k-ϵ model is capable of predicting the instability of the bedwaves of the open channel. The unstable condition predicted by the model agrees fairly well with the existing experimental results. The analysis also physically explained the migration directions of the bedwaves. The instability and migrating mechanism is explained by the phase shift of the bed elevation and the net erosion rate.

Under the effect of density stratification, the unstable region disappears in the range of large wavenumber in the vicinity of the critical Froude number. It is suggested that the decrease of the eddy viscosity produces a change in phase difference, resulting in the stabilization of the short wavelength bedwaves.

In Chapter 3, the bed instability generated by the turbidity currents is investigated. In this analysis, the mixing length model is used to account for the turbulent closure. We assume turbidity currents possesses an equilibrium state at the lower layer near to the bottom in which the suspended sediment concentration is very high.

In turbidity currents, the dimensionless settling velocity is a very important parameters which causes stratification and affects the flow structures. In the base state solution, the suspended sediment concentration in the depth direction is almost uniform when the settling velocity is small. As the settling velocity increases, the profile deviates from the uniform distribution. The concentration increases at the bottom and decreases at the upper part. It is also found that the flow velocity at the upper part decreases when the settling velocity increases.

As pointed out earlier, the settling velocity is a very sensitive parameter in the case of turbidity current. In the case of settling velocity is greater than 0.08, the normal flow condition of the turbidity current is expected to no longer exist. In this condition, the suspended sediment concentration turns to be zero at the density interface.

The results of the linear stability analysis shows that the bed becomes unstable when the densimetric Froude number is approximately 0.4. In the vicinity of the critical Froude number, the predicted bedwaves are in the range of wavenumber 1.0 to 1.5, and reduce to smaller range of 0.1 to 1.0 at high value of Froude number. In addition, the shape of the unstable region when the settling velocity is equal to 0.08 is strange which does not possess of any physical implications.

Bibliography

R.A. Bagnold. Auto-suspension of transported sediment: Turbidity currents. *Proceeding of Royal Society of London, A,.*, 265, 1962. doi: 10.1098/rspa.1962.0012.

M.I. Cantero, S. Balachandar, A. Cantelli, C. Pirmez, and G. Parker. Turbidity current with a roof: Direct numerical simulation of self-stratified turbulent channel flow driven by suspended sediment. *J. Geophys. Res.*, 114, 2009. doi: 10.1029/2008JC004978.

N. L. Coleman. Effects of suspended sediment on the open-channel velocity distribution. *Water Resour. Res.*, 22:1377–1384, 1986.

M. Colombini. Revisiting the linear theory of sand dune formation. *J. Fluid Mech*, 502:197–20, 2004.

F. Engelund. Instability of erodible beds. *J. Fluid mech*, 42(2):225–244, 1970.

J. Fredsoe. On the development of dunes in erodible channels. *J. Fluid mech*, 64 (1):1–16, 1974.

Y. Fukushima and N. Hayakawa. Analysis of inclined wall plume by the k-ϵ turbulence model. *Journal of Applied Mechanics*, 57, 1990. doi: 10.1115/1.2892011.

M. Garcia and G. Parker. Entrainment of bed sediment into suspension. *J. Hydraul. Eng, ASCE*, 117(4):414–435, 1991.

M.O. Garcia and D.M. Hull. Turbidites from giant hawaiian landslides: results from ocean drilling program site 842. *Geology*, 22, 1994.

H.P. Guy, D. B. Simons, and Richarson E.V. Summary of alluvial channel data from flume experiments 1956-1961. *Journal of Sedimentology*, 462-I, 1966.

B.C. Heezen and W.M. Ewing. Turbidity currents and submarin slumps, and the 1929 grand banks [newfoundland] earthquake. *American Journal of Science*, 250(12), 1952. doi: 10.2475/ajs.250.12.849.

N. Izumi. The formation of submarine gullies by turbidity currents. *J, Geophys. Res.*, 109, 2004. doi: 10.1029/2003JC001898.

J. F. Kennedy. Stationary waves and antidunes in alluvial channels. Rep. no kh-r-2, w. m keck laboratory of hydraulics and water resources, California Institute of Technology, Pasadena, California, 1961.

J.F. Kennedy. The mechanism of dunes and antidunes in erodible-bed channels. *J. Fluid Mech.*, 16, 1963.

B. Kneller and C. Buckee. The structure and fluid mechanics of turibidity currents: a review of some recent studies and their geological implications. *Sedimentology*, 47, 2000. doi: 10.1046/j.1365-3091.2000.047s1062.x.

D.R. Lowe. Sediment gravity flow: Ii. depositional models with special reference to the deposits of high-density turbidity currents. *J. Sedim. Petrol*, 52, 1982.

R. Luchi, G. Parker, S. Lalachandar, and K. Naito. Mechanism governing continuous long runout turbidity currents. *Anuual Journal of Hydraulics Engineering, JSCE.*, 71, 2015.

G.V. Middleton. Sediment deposition from turbidity currents. *Ann. Rev. Earth Planet, Sci.*, 21, 1993.

G. Parker. Conditions for the ignition of catastrophically erosive turbidity currents. *Marine Geology,.*, 46, 1982.

G. Parker, Y. Fukushima, and H.M. Pantin. Self-acelerating turbidity currents. *J. Fluid Mech,.*, 171, 1986.

D.J.W. Piper, P. Cochonat, and M. Morrison. The sequence of events around the epicenter of the 1929 grand banks earthquake: initiation of debris flows and turbidity currents inferred from sidescan sonar. *Sedimentoloy*, 46, 1999.

K. J. Richards. The formation of ripples and dunes on an erodible bed. *J. Fluid Mech*, 99(4):597–618, 1980.

O.E. Sequeiros, A. Cantelli, E. Viparelli, J.D.L White, M.H. Garcia, and G. Parker. Modeling turbidity currents with nonuniform sediment and reverse buoyancy. *Water Resources Research*, 45, 2009. doi: 10.1029/2008WR007422.

P.J. Talling, R.B. Wynn, D.G. Masson, M. Frenz, B.T. Cronin, R. Schiebel, A.M. Akhmetzhanov, S. Dallmeier-Tiessen, S. Benetti, P.P.E Weaver, A. Georgiopoulou, C. Zuhlsdorff, and L.A. Amy. Onset of submarine debris flow deposition far from original giant landslide. *Nature*, 450, 2007c. doi: 10.1038/nature06313.

P.P.E. Weaver, R.G. Rothwell, J. Ebbing, and D. Gunn. Correlation, frequency of emplacement and source directions of megaturbidites on the madeira abyssal plain. *Mar. Geol*, 109, 1992.

J. C. Winterwerp. Stratification effects by cohesive and noncohesive sediment. *J. Geophys. Res.*, 106:22,559–22,574, 2001.

J. C. Winterwerp. Stratification effects by fine suspended sediment at low, medium, and very high concentrations. *J. Geophys. Res.*, 111:2156–2202, 2006.

L.D. Wright, W.J. Jr. Wiseman, Z.S. Yang, B.D. Bornhold, G.H. Keller, D.B. Prior, and J.N. Suhayda. Processses of marine dispersal and deposition of suspended silts off the modern mouth of the juanghe (yellow) river. *Cont. Shelf Res.*, 10, 1990.

T. Yeh and G. Parker. Software for evaluating sediment-induced stratification in open-channel flows. *Comput. Geosci.*, 53, 2013.